A method for the assessment of the wind induced natural ventilation forces acting on low rise building arrays

B.E. Lee, M. Hussain and B. Soliman

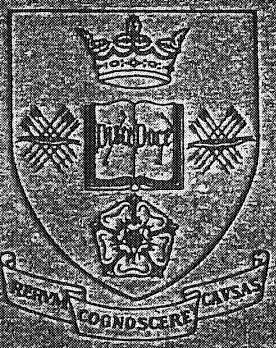

Department of Building Science
Faculty of Architectural Studies
University of Sheffield
March 1979

CONTENTS

NOTATION

A	area of a leakage aperture
A_b	area of leakage apertures on the leeward face and sides of a building
A_r	area of leakage apertures on the roof of a building
A_w	area of leakage apertures on the windward face of a building
A_f	frontal aspect ratio of building models, l1/36
A_s	side aspect ratio of building models, l2/36
C_i	infiltration coefficient
C_{pb}	average pressure coefficient acting on leeward face and sides
C_{pe}	general external face pressure coefficient
C_{pi}	general internal pressure coefficient
C_{pir}	internal pressure coefficient for leakage apertures in vertical faces and roof
C_{pis}	internal pressure coefficient for leakage apertures in vertical faces only
C_{pw}	average pressure coefficient acting on windward face
C_s	roof suction coefficient, non-dimensionalised by velocity at roof height
C_{s1}	average roof suction coefficient
ΔC_{p1}	pressure difference coefficient acting across windward and leeward faces of building,
ΔC_{pr}	pressure difference coefficient acting across roof of a building
E_d	downstream flow reattachment distance behind a building
E_t	$E_u + E_d$
E_u	upstream flow separation distance in front of a building
E_v	maximum separation distance between buildings for the existence of a stable vortex
H	building height

L_c	crack length
l_1	frontal aspect ratio model length variable, transverse dimension normal to flow, mm.
l_2	side aspect ratio model length variable, longitudinal dimension parallel to flow, mm.
n	exponent in infiltration rate equation
p_e	external pressure
p_i	internal pressure
Δp	pressure difference acting across windward and leeward faces of a building
Δp_o	pressure difference acting across an opening or infiltration gap in a vertical wall
Δp_r	pressure difference acting across an opening or infiltration gap in the roof
Q	ventilation rate
R	upstream fetch length
S_c	clear spacing in the flow direction between buildings in an array
V_g	gradient wind speed
λ_p	array plan area density
ρ	air density
θ	wind direction

All of the pressure coefficients, with the exception of C_s, have been formed by normalising pressures with respect to a dynamic head based on the free stream or gradient wind speed.

1. INTRODUCTION

Ventilation, in terms of supplying fresh outside air into building interiors, is one of several means by which the indoor climate of a building may be controlled. Introducing outside air internally may be achieved by means of natural ventilation, mechanical ventilation or air-conditioning. The choice of method has its consequence not only on the architectural design principles, but also on the building cost and the resulting indoor environment. Mechanical ventilation, which may be necessary in some buildings, will involve additional expenditure and increased running costs and may be compensated for economically. The artificial control of ventilation will enable conditions very close to the required internal environment to be attained, in contrast with the natural methods of ventilation which rely on highly variable external climatic conditions. However, in most cases, where the external climatic impacts are not too severe to produce balanced conditions by natural means and when minimum building cost is of prime importance, natural ventilation becomes the only available alternative for the designer. It may also be noted that the consumption of energy for heating purposes in housing in many countries represents a large proportion of the national energy budget, a considerable part of which is wasted by uncontrolled excessive ventilation. Therefore a proper estimate of the natural ventilation rates in buildings is necessary if buildings are to meet both their environmental and economic requirements.

Natural ventilation occurs in virtually all buildings through the openings in their envelope. Intentional air flow through openings provided in the building, such as windows or ducts is usually referred to as ventilation. On the other hand, unintentional flow may occur through gaps and cracks in the building such as those round windows and doors, this type of flow being known as infiltration. Whereas ventilation may be allowed or prevented through controlling the ventilation openings, infiltration is usually uncontrolled and subject to the variability of the natural forces created by the ambient climatic conditions. However, infiltration rates may be minimised if the gaps and cracks round ventilation openings and doors are sealed as far as is practicable.

The main principle that operates to produce natural ventilation in buildings is the existence of a pressure difference between the inside and the outside of the building. The magnitude of the pressure difference and of the flow resistance will determine the rate of air flow through the openings. The size, shape and location of openings determine the speed and pattern of internal flow. The two forces that produce pressure differences across building elements are the wind force and the thermal force, known as the "stack effect". For the low rise buildings which are the subject of this study the stack effect is considered to be negligible in comparison with the effects of wind pressure forces.

Ventilation may also occur, though to a lesser extent, either due to pressure fluctuations on the walls, an action related to the turbulent nature of the wind, or due to turbulence diffusion. Although the magnitude of ventilation provided by these two mechanisms is normally considered to be negligible, there is insufficient information currently available by which to quantify it.

2. EXISTING METHODS FOR THE PREDICTION OF INFILTRATION RATES

2.1 The Crack Method

The two widely used methods of predicting natural ventilation or infiltration rates in buildings are the air change method and the crack method. Both methods are described in the IHVE Guide (1970) and the ASHRAE Guide (1972). The air change method, which is entirely empirical, is based on the assumption that similar building types of typical construction and normal use in winter would have similar infiltration rates.

The crack method for infiltration calculation is based in principle on the following equation which relates the ventilation rate, Q, to the pressure difference, Δp_o, acting across any opening,

$$Q = C_i . L_c \ (\Delta p_o)^{1/n}$$

For a particular building, the infiltration coefficient, C_i, and the crack length, L_c, are dependent on the type and the size of the openings. From the work on air flow through openings, a relationship has been shown to exist between C_i and the exponent n, Bilsborrow (1973). Therefore, it remains to determine Δp_o in the equation in order to obtain the ventilation rate, Q. From the work on air flow round building models an estimate of the mean pressure difference across the building Δp, may be obtained, half of which is assumed to act across each of the windward and the leeward faces of the building, giving Δp_o. The main assumption made in the existing guides for the estimation of the mean pressure difference across any building, Δp, (hence Δp_o) is that Δp is approximately equal to the velocity pressure of the wind at the roof top level. Therefore, if the design wind speed and mean velocity profile of the wind are assumed, the corresponding velocity pressure profiles may be plotted. These velocity pressure profiles may then be used to obtain Δp for buildings of any given height for the terrain conditions implied by the velocity profile choice. It appears that the main assumption made in the guides for the estimation of Δp may result in considerable error since a number of important factors affecting Δp are neglected. These factors include definitions of the building form and the properties of the oncoming flow. The effect of these factors is well documented (see for example the BSI Wind Loading Code of Practice CP3, Chapter V, part 2 (1972) and the work of Jensen and Franck (1965)).

There are two further factors concerning the existing methods of infiltration rate prediction which should be mentioned. The first of these is that they are based on studies relating to the exposure of only isolated tall buildings to the wind, see for instance Jackman (1969), and cannot be

adequately adapted to the multiple low rise building problem. Secondly there is no allowance within these methods for infiltration via the roof, though this is of considerable importance for low rise housing in some areas of the world. It is important therefore to re-consider the factors affecting Δp if a reliable estimate of the ventilation rate is to be made.

2.2 The factors affecting the pressure difference across buildings

There are a large number of variables affecting the pressure difference across buildings in the natural wind. The complexity of interaction between these variables and the difficulty of controlling them in nature has given rise to the dependence on scale model experimental work as the main source of information. In particular the work done on the drag, and hence Δp, of bluff bodies immersed in turbulent boundary layers provide the basic information required, see for example the work of Good and Joubert (1968), Jensen and Franck (1965), Morris (1955), Joubert, Perry and Stevens (1971) and Wooding, Bradley and Marshall (1973). From this work the similarity between wind flow over the earth's surface and the turbulent boundary layer flow over rough surfaces has been established. Hence, buildings on the earth's surface may be considered as elements on a rough surface over which a turbulent boundary layer flows.

By definition, the drag exerted on any bluff body in boundary layer flow is the difference between the integral of the windward and the leeward surface pressure distributions. These pressures are determined by the process of separation and reattachment of air flow round the body. Although the factors affecting separation are not necessarily the same as those affecting reattachment, it seems logical to classify all the factors involved into the following two groups:

(a) factors related to the building form, and

(b) factors related to the properties of the wind.

The main properties of form known to affect the drag of buildings in urban areas are the individual form and the form of the group in which individual buildings are situated. Individual building form may then be broken down to building shape, building size and building permeability.

In the case of low building density where buildings are wide apart, i.e. in open country, the individual building form is the only form that the wind can 'see'. As the density increases, i.e. in suburban and urban areas, buildings are close to each other so that each building form becomes a detail in the group form as a whole. In this

case the group form becomes more important than the individual building form in influencing the drag forces experienced by each building. Recent experimental work (see for example Joubert, Perry and Stevenson (1971) shows how the group geometry of roughness elements simulating buildings immersed in turbulent boundary layer flow affect the drag force on each element.

2.3 The form of the present investigation

In the discussion so far, the problem of making a reliable estimate of the value of the wind pressure forces for natural ventilation calculations is shown to depend on two main groups of factors, i.e. form-related factors and flow-related factors. Thus, in urban areas where buildings occur mainly in groups, it is expected that the three main factors affecting Δp are (i) the building geometry, (ii) the group form and (iii) the properties of the natural wind.

If the properties of the wind structure in the atmospheric boundary layer flow over suburban terrain are assumed, on the basis of previous full scale measurements, and if these properties can be adequately modelled in a wind tunnel, it should then be possible to conduct a series of detailed measurements to establish the existence of a set of relationships between the wind-induced pressure forces on a building and the form factors which describe the building and its immediate surroundings. It is the intention of this paper to demonstrate that such a set of relationships may be determined.

3. THE EXPERIMENTAL PROCEDURE

3.1 The Wind Tunnel and Incident Flow

The series of experimental tests, to be described below, were conducted in the Sheffield University 1.2 x 1.2 m boundary layer wind tunnel. The wind tunnel has a working section 7.2 m long whose cross section measures 1.2 x 1.2 m, incorporating a 1.1 m diameter turntable and whose centre lies 5.4 m downstream of the entry position.

The method used for the simulation of the suburban terrain atmospheric boundary layer utilises the fence, spires and floor roughness element approach suggested by Counihan (1973). This use of Counihan's method has been shown to give an adequate representation of both the mean velocity and turbulence characteristics appropriate to flow over suburban terrain conditions, Lee (1978). The detailed characteristics of this simulated boundary layer, having a power law exponent of 0.28 and a boundary layer height of 800 mm are also given by Lee (1978). The linear scale factor of the boundary layer simulation based on spectral analysis methods is 1:350. This simulated atmospheric incident flow was subsequently modified by the flow characteristics produced by a particular model building group layout pattern in the immediate vicinity of an instrumented central model building. The compromise between the size of the model building array and the use of the simulated atmospheric flow apparatus is discussed later.

Full details of the experimental procedure and of its results can be found in Hussain (1979).

3.2 The Test Programme

Throughout the test programme pressures were measured on a range of instrumented model buildings which were positioned at the centre of arrays of identical models. These central models were fitted with pressure tappings on their windward and leeward faces and their roofs. The overall investigation was conducted in 3 phases as follows:

Phase 1 Cuboid models

Dimensions: 20mm cubes and 36mm cubes

Array patterns: Normal (gridiron)
Staggered (checkerboard)
Random

Array plan area density : 3.1% to 50% (13 values)

Wind directions : $0^{\circ} < \theta < 90^{\circ}$

Phase 2 Frontal Aspect Ratio models

Dimensions: Front face 36mm x l_1, Side face 36 x 36mm

where l_1 = 18, 36, 54, 72 and 144 mm

Array pattern : Normal (gridiron)

Array plan area density : 2.5% to 60% (15 values)

Wind direction : $\theta = 0^{\circ}$, wind normal to front face

Phase 3 Side Aspect Ratio models

Dimensions : Side face 36mm x l_2, front face 36 x 36mm

Array pattern : Normal (gridiron)

Array plan area density : 2.5% to 60% (15 values)

Wind direction : $\theta = 0^{\circ}$ wind normal to front face

Throughout the presentation and discussion of the results the model surface pressures are referred to in coefficient form, non-dimensionalised with respect to the free stream velocity which approximates to a gradient wind speed in full scale. In the tests included in phase 1 of the investigation a study was made of the influence of the size of the array, the results of which were then applied to phases 2 and 3. A wide range of velocity profile measurements were made in order to investigate the characteristics of the inner boundary layer flow which grew over the model building arrays.

3.3 The Definition of Housing Density

The design and planning of residential areas often refers to housing density as an indicator of environmental quality. This follows from the hypothesis that the geometry of urban form will largely determine its environmental conditions. Since the density of built form is a function of its geometry it is important to determine the relation between the geometrical parameters needed to define group form and its density.

Several studies have been made in which the density of residential areas were considered in relation to planning parameters as well as geometrical parameters for different environmental criteria. A review on these studies has been made in order to see how accurately group form can be defined in terms of the parameters considered, as well as to determine the practical limits of these parameters. A theoretical analysis has also been presented to enable a complete definition of group form to be made, in terms of a proposed set of geometrical parameters and group density.

Further details of this aspect of the overall study

are available in Soliman and Lee (1974). The conclusion reached was that in order to achieve complete definition of group geometry, the frontal and side aspect ratios together with the ratio of building length to site length in both directions were required as well as the cotan of the angle of obstruction in both directions. Equations were given for the general relation between these parameters in terms of either the plan area density or the frontal area density. Accordingly, array plan area density has been used in this paper as the major determinant of a group form for a particular building geometry.

4. THE RESULTS AND DISCUSSION

4.1 The Influence of the Array Size and Upstream Fetch

At the start of the investigation on arrays of model buildings a series of tests were performed in order to determine the influence of upstream fetch geometry on the model buildings surface pressure distributions. The extremes of upstream fetch conditions were either that the particular model array under test could be arranged to fill the entire length of the working section, or that the general roughness array of the atmospheric boundary layer simulation apparatus could extend down to the immediate proximity of a small particular array size. However it was felt that some compromise would exist whereby it was possible to have a sufficiently large array size to yield representative results and at the same time to have the correct general background to the flow field conditions that would be produced by the atmospheric flow simulation apparatus. This part of the investigation, which utilised only the cube form of model building, was conducted for plan area densities of 5%, 10% and 20% in the normal (gridiron) layout pattern and 10%, 20% and 25% in the staggered (checkerboard) pattern, and only for the $\emptyset = 0^{o}$ wind direction.

The first tests were carried with only the model array, for a particular value of plan area density, in the wind tunnel working section, where the fetch length of this array, R, could be varied from 3H to 145H upstream of the central instrumental model and 3H to 25H downstream. The test results, shown in Figure 1, indicate that the reduction of the pressure coefficient drop across the building, ΔC_{p1}, produced by increasing fetch length is also dependent on the pattern type and plan area density of the array. The figure shows that the majority of this reduction has occurred for fetch lengths of R = 25H for the low density arrays, 5% density in the normal pattern and 10% density in the staggered pattern, and for R = 10H in the higher density arrays, 20% normal and 25% staggered patterns.

Following this assessment of the influence of array size alone on the pressure forces on the central model the simulated atmospheric boundary layer apparatus was then placed in the upstream part of the working section. A further reduction in the value of ΔC_{p1} was then recorded for all the combinations of array pattern and plan area density considered. As an example of this further reduction, the value of ΔC_{p1} for the 5% density normal pattern fell from 0.25 and 0.17 for fetch lengths of 25H and 145H respectively to a value of 0.15 for the combination of a 25H array fetch with the atmospheric boundary layer simulation upstream. This reduction is considered to justify the use of a particular upstream model array fetch of 25H for low density arrays reducing to 10H for the highest density arrays later in the test programme. The simulation apparatus then remained in the forward part of the working section for the remainder of the

test programme. Hence, the authors were satisfied that the wind tunnel tests would be performed in model terrain conditions which would simulate those appropriate to wind action on large groups of low rise buildings in suburban areas.

4.2 The Area of Influence

The array of model buildings which surround the central model has its size dictated by the upstream fetch limits described in the previous section. These upstream limits were also used for the downstream fetch length definition. The array size to either side of the model was such as to fill the working section width, 1.2 m, being 16H each side for the 36 mm high cuboid models.

However it was considered of some interest to attempt to define the exact area of surrounding buildings whose positions exerted an influence on the value of ΔCp_1 of the central model. This exercise was performed only for a 10% plan area density pattern of cuboid models. By keeping the central model normal to the flow and by setting the surrounding normal pattern layout at various angles to the flow, a superposition of the results represents those appropriate to a random layout pattern at this plan area density. The tests then took the form of removing successive members of the model array and noting the effects on the central model surface pressures. The results are presented in Figure 2 where the areas of influence which induce changes of greater than $\pm$ 5% and $\pm$ 10% in the value of ΔCp_1 are shown. This figure demonstrates the relative importance of upwind and downwind fetch lengths and shows that the effect of buildings in the side sectors is negligible.

4.3 The Influence of the Array Form on Model Surface Pressures

When turbulent flow occurs over a rough surface composed of discrete roughness elements it is possible to describe the existence of a number of flow regimes which are governed by the way in which the layout of elements occurs. These flow regimes, which were suggested by Morris (1955) and whose existence for some types of three-dimensional roughness element has been confirmed by Lee and Soliman (1977) are denoted as isolated roughness flow, wake interference flow and skimming flow.

In the isolated roughness flow regime, Fig. 3(a), the roughness elements are sufficiently far apart that each element acts in isolation and behind which the wake and separation bubble develop completely, flow reattachment to the surface occurring before the next element is reached. Here the clear spacing in the flow direction between adjacent elements, Sc, is greater than E_t, the sum of the upstream separation distance, Eu, and the downstream distance, Ed. In the third category, the skimming flow regime, Figure 3(c),

the roughness elements are now sufficiently close together that a stable vortex can form in the space between the elements and the flow appears to skim on their crests. Here the separation distance between elements is less than E_v, the maximum gap size for the existence of such a stable vortex. The wake interference regime, Figure 3(b), then exists between these other regimes where the separation bubble does not have sufficient space to develop fully but where the distance is too large for a stable vortex to remain. Here the clear spacing lies between E_t and E_v.

4.3.1 The Cuboid Model Tests

The measurements of the mean surface pressure forces were first carried out on the cuboid models for the ranges of parameters described in Section 3. Figure 4, which presents these results, shows the variation of ΔC_{p1} with element clear spacing ratio S_c/H, and plan area density λ_p, for both the normal and staggered patterns. These results are shown to be represented by broken straight line relationships for both layout patterns considered, where break points are considered to reflect a change from one flow regime to another, as described in the previous section.

From this figure the following conclusions are suggested:

a) The isolated roughness flow regime exists for values of $S_c/H > 2.4$ for both layout patterns.

b) The wake interference flow regime exists for values of $1.4 < S_c/H < 2.4$.

c) The skimming flow regime exists for values of $S_c/H < 1.4$ for both layout patterns.

Figure 4 also shows the value of ΔC_{p1} for an isolated cuboid model building in the simulated atmospheric flow. A comparison of this value with those for the pressure drop across grouped buildings clearly illustrates the importance of building proximity effects in the determination of wind pressure forces and hence wind induced ventilation rates.

In addition to the measurements of the windward and leeward wall pressures, the roof pressure distributions were also measured and were subsequently integrated to give the mean roof suction force. The variation of the roof suction coefficient, C_{S1}, with decreasing element clear spacing, Figure 5, showed no apparent change which might correspond to the change of flow regime from isolated roughness flow to wake interference flow. However the data indicated that skimming flow is characterised by an approximate constant value of the suction force for all the element spacing values tested in this regime.

The behaviour of both the wall pressures and roof pressures with respect to the variation of array plan area

density have been found to be similar for both the normal and staggered layout patterns. The trends indicated for the wall pressure variations for increasing plan area densities in both the patterns give approximately parallel lines in the first two flow regimes, suggesting the spacing parameter to be the governing factor rather than the pattern format. In the skimming flow regime, however, figure 4 indicates that the plan area density is the more important parameter. In view of this, only the normal pattern has been considered in the tests on other building forms.

4.3.2 The Frontal Aspect Ratio Variation Tests

The variation of the central model pressure drop coefficient, ΔCp_1, with variations in array model clear spacing for the range of frontal aspect ratio models from $A_f = 0.5$ to $A_f = 4.0$ is shown in Figure 6. The inflection points in the relationship between the model pressure drop coefficient and the clear spacing ratio, similar to those found for the cuboid models, suggests that the values of Sc/H at which the flow regime changes occur depends not only on the model spacing but also on the value of the model's frontal aspect ratio. Across the range of frontal aspect ratio from 0.5 to 4.0 it can be seen that the change of flow regime from isolated roughness flow to wake interference flow occurs at values of Sc/H which progress from 2.25 to 3.0 respectively. Similarly, the values of Sc/H at which the second change occurs also increases from 1.30 to 1.55 across the same range of frontal aspect ratio models.

Figure 7 shows the variation of the roof suction coefficient with model clear spacing for the range of frontal aspect ratio models tested. The change in the pattern of suction coefficient variation is similar to that described earlier for groups of cuboid model buildings.

4.3.3 The Side Aspect Ratio Variation Tests

Figure 8 shows the variation of the model pressure drop coefficient, ΔCp_1, with the model clear spacing, Sc, for values of the side aspect ratio models of $A_s = 0.5$, 1.0, 1.5 and 2.0. The inflection points in the rate of reduction of model pressure drop with spacing have again been used to identify the changes of flow regimes. The first change from the isolated roughness to wake interference flow regimes occurs at values of Sc/H varying from 2.1 to 2.6 as the side aspect ratio is increased from 0.5 to 2.0. The second change from the wake interference to the skimming flow regime occurs at a constant value of Sc/H of 1.4 for all model side aspect ratio array values. The variation of roof suction coefficient for varying side aspect ratio models is shown in Figure 9.

4.4 The Fetch Length Correction

The influence of upstream fetch on the surface pressures acting on the central model, for arrays of cubes, has been dealt with in section 4.1. Here it was found that the model group fetch size required for the surface pressures to stabilise at their minimum value varied from 10H to 25H and was dependent also on the group plan area density, for groups of buildings situated within a suburban terrain atmospheric boundary layer. From these tests it was found that if the fetch length was too short for the conditions of pressure stabilisation to occur then this would result in an increase in the surface pressure forces. It has, thus, been possible, using the results of all the tests on the influence of upstream fetch length, to produce a family of curves for each of the flow regimes indicating the increase in surface pressure difference which is consequent upon the existence of short fetch lengths. Such a family of curves is shown in figure 10 depicting the variation of ΔC_{p1} with R/H, and is considered to be applicable to all individual model shapes.

4.5 The Influence of Wind Direction on the Vertical Wall Pressures

The data on the influence of wind direction on the surface pressures acting on groups of low rise buildings stem from an earlier series of tests, reported by Soliman (1976), on groups of cuboid models in normal, staggered and random layout patterns. It is interesting to note that Dick (1949), in his full scale studies of the natural ventilation of houses, considered that wind direction was of negligible effect. However this particular conclusion may not be generally applicable particularly where ventilation openings are considered on two opposite faces of the building only, i.e. the windward and leeward faces for wind direction $\theta = 0^{o}$. For wind directions other than $\theta = 0^{o}$ the effective ventilation pressures for ventilation openings on all four sides of the building may be estimated by vectorial summation of the results presented here, an example of which is given later.

The variation of ΔC_{p1} with the model orientation, θ, is shown in Figure 11 for the two layout patterns and for three values of the group plan area density. A comparison with the corresponding data for an isolated cuboid model is also presented.

The behaviour of these curves may be explained, with reference to section 4.3, by classifying the flow regimes which correspond to the various values of plan area density. At a layout density of 9.2% this is an isolated flow regime where the type of incident flow dominates the model behaviour and pattern type is less important. However, at a layout density of 18.9% the flow regime is wake interference flow. Here it is suggested that the model behaviour will be dominated by the wake of the blocks upstream which forms the boundary layer structure over the element layout itself, Perry, Schofield and Joubert, (1969), and hence the results will be grouped

now by layout pattern and the influence of the upstream flow type is subordinate. Finally, at a layout density of 39.1% this is a skimming flow regime. Here the incident flow skims on the crests of the elements and the surface pressures induced by the cavity vortex remain almost constant.

The effect of model orientation on the value of ΔC_{p1} in the range of $0^o < \theta < 60^o$ is shown to be negligible for the values of density considered, tending to confirm the finding of Dick from his full scale studies.

In order for the effect of building orientation angle to be applied to the prediction of ventilation rates the results obtained for ΔC_{p1} at different values of θ and group plan area density given in Figure 11 have been normalised with respect to their values at $\theta = 0^o$. A plot of these normalised values for the two layout patterns in all three flow regimes is given in Figure 12. This figure indicates that all the results, regardless of layout pattern or flow regime, fall approximately onto a single curve .

This finding from figure 12 is most important since it now enables the wind directional characteristics to be considerably simplified in a design procedure. Figure 13 has been compiled from Figure 12 and incorporates the directional correction necessary to convert the value of ΔC_{p1} for flow normal to model, on the vertical axis, to the corresponding value appropriate to the required value of θ, on the horizontal axis.

4.6 The Roof Suction

This section deals with the procedure necessary to quantify the roof suction coefficients for low rise flat roofed buildings which form part of a large array, and follows closely the steps outlined in the preceding sections of this paper.

During the initial tests on the influence of upstream array fetch length, the variation of the roof suction coefficient was found to be the same as that of the side wall pressures. Thus since the roof suction was found to stabilise at minimum values for the fetch lengths already discussed it had been considered appropriate to apply the form of the wall pressure fetch length correction, figure 10, to the roof suctions, figure 14.

Since the effect of wind direction on the vertical wall surface pressures of arrays of cuboid model buildings, Soliman (1976), had not been extended to a comparable study of roof suctions, it had been found necessary to utilise trends given by other authors for isolated building models.

The roof pressure distributions on a surface mounted cube in smooth flow conditions, given by ESDU 71016 (1971) were analysed, and it was found that the roof suction

coefficient, C_S, averaged along the centre line of the cube varied very little with wind direction. The values of the average centre-line roof suction coefficient for orientation angles 0^o, 15^o, 30^o and 45^o were found to be -0.59, -0.51, -0.58 and -0.41 respectively. Furthermore, when the average value for the roof suction coefficient along a diagonal line was calculated for various wind directions its value was found to be more uniform at -0.59, -0.63, -0.58 and -0.56 respectively. Similar observations have also been reported by Tieleman and Reinhold (1976) from their wind tunnel model investigations for 32 geometries of isolated buildings in a simulated atmospheric boundary layer.

On the basis of these observations, it is suggested that the effect of orientation angle will be negligible over the total roof suction and that no correction is required. If, however, the ventilation openings are not distributed evenly over the entire roof and are located only in one particular section then the appropriate wind tunnel data will have to be reffered to, i.e. ESDU 71016 (1971), and a correction may be applied.

5. THE PREDICTION METHOD

In the introductory remarks to this paper the importance of various definitive parameters in the prediction of low rise building ventilation rates was hypothesised. The presentation of the results of this experimental investigation has attempted to demonstrate how the form of a building and the form of the group in which it is situated, the conditions of upstream fetch and the direction of the wind all contribute an influence on the surface pressures experienced by the building and hence all play some part in determining the resultant ventilation rate.

5.1 The Prediction of Vertical Wall Pressure Coefficients

Having seen the effect of the important parameters which influence the value of the vertical wall pressure difference coefficient, ΔC_{p1}, a prediction procedure for low rise buildings is now possible. Assuming the buildings to be of similar heights in a group, a chart can be constructed by placing figures 6, 8, 10 and 13 side by side, as shown in figure 15. This chart can then be used to calculate the pressure difference across two opposite faces of buildings. It is applicable to buildings of varying frontal aspect ratio, having a fixed value of their side aspect ratio of 1, as well as for buildings of varying side aspect ratios with a fixed frontal aspect ratio of 1. The proportions of these structures are considered to cover a wide range of low rise building forms in current use.

The value of ΔC_{p1} for buildings of varying frontal or side aspect ratio can be determined from either of the first two parts of the chart, given the group clear spacing in the flow direction, to which a correction can then be applied from the third section of the chart if the fetch length is smaller than 25H. The required value of ΔC_{p1} across the building for any wind direction may then be obtained from the last section of the chart.

If the building contains infiltration openings on all four vertical faces the necessary values of ΔC_{p1} may be obtained by using the chart twice. As an example of this, if a building of Af = 2.0 were set at $\theta = 15^{\circ}$ to the flow direction, the value of ΔC_{p1} between the two rectangular faces which were approximately windward and leeward could be simply read from the chart. The value of ΔC_{p1} between the other pair of square faces could then be read from the chart as $A_s = 2.0$ for $\theta = 75^{\circ}$.

Two separate examples showing the sequence of these steps are indicated on figure 15. In example 1 the building has proportions defined by $A_f = 1.5$ and $A_s = 1.0$ and is part of a large array, R/H>25, characterised by a clear spacing

of 3.0H, with the flow direction at 60^{o} to the front face. The appropriate value of ΔC_{p1} can thus be determined as 0.104, acting across the front and rear faces. The corresponding value of ΔC_{p1} acting across the side faces in this example could then be determined by using the second plot for a value of As = 1.5 and a value of $\theta = 30^{o}$, giving a pressure difference coefficient of 0.138. In the second example shown in figure 15 the wind direction chosen is $\theta = 0^{o}$ and thus since the side faces are now both parallel with the flow no pressure difference will exist between them.

5.2 The Prediction of the Roof Suction Coefficients

In a similar manner to that described in section 5.1 for the vertical wall pressure coefficients, it is now possible to construct a chart for the prediction of roof suction coefficients. This has been performed in figure 16 by placing figures 7, 9 and 14 together and again shows two examples of the sequence of steps necessary to determine a value for C_{s1}. For the reasons explained in section 4.6, no directional correction factor has been included since C_{s1} is an average value applicable to the roof as a whole.

This chart depicted in figure 16 allows the external pressure on the roof to be determined for a given set of conditions. However, in order to determine an infiltration rate through an aperture in the roof the corresponding value of the buildings internal pressure will be required, since

$$\Delta pr = \Delta C_{pr} \cdot \tfrac{1}{2} \rho V_G^2$$

$$= (C_{s1} - C_{pir}) \cdot \tfrac{1}{2} \rho V_G^2$$

where Δpr is the pressure difference across an opening in the roof, C_{s1} is the roof external pressure coefficient determined from figure 16 and C_{pir} is the internal pressure coefficient calculated for the condition where apertures exist in the roof. Appendix A describes the procedure for the determination of C_{pir} for given conditions of building and group form and for a range of values of aperture areas on the vertical walls and the roof.

An example of the use of figure 16, used to predict a value of C_{s1}, together with the determination of the appropriate value of C_{pir} is given in Appendix A.

5.3 The Application of the Prediction Method

The prediction method has enabled an estimate of ΔC_{p1} and ΔC_{pr} to be made which takes account of some of the more important form factors which are thought to influence it. Since ΔC_{p1} is defined as

$$\Delta C_{p1} = \frac{\Delta p}{\tfrac{1}{2} \rho V_G^2}$$

and ΔC_{pr} is defined as

$$\Delta C_{pr} = \frac{\Delta pr}{\frac{1}{2} \rho V_G^2}$$

it requires only a knowledge of VG, the gradient wind speed, in order to determine Δp, and hence Δpo and Δpr. These two pressure difference terms, Δpo and Δpr, may then be applied directly to the determination of an infiltration rate by insertion in the equation

$$Q = Ci.Lc \left(\Delta_{po} \right)^{1/n}$$

discussed in section 2.1, whilst a corresponding equation in Δpr exists for the calculation of the roof infiltration rate.

The data for gradient wind speeds over the United Kingdom are presented in Appendix B where their use in this prediction procedure is discussed. A significant advantage of this procedure is that it is not necessary to involve an estimate of the wind velocity at the building roof height, an especially difficult procedure where the average roof height of an array of low rise buildings may be below the standard meteorological reference height. However, as Appendix B points out, this independence of the roof height velocity is an assumption which is only valid if the ratio of building height to boundary layer thickness is small.

The gradient wind speed data are available based on a choice of three probability conditions, i.e. these speeds exceeded for 50%, 10% or 1% of the time, figures B1 to B3. The choice of probability condition and hence the value of the gradient wind speed chosen must depend on the use to which the data is to be applied.

If ventilation rate calculations are to be performed in order to determine average internal air change rate conditions for odour and fume removal then the applicable condition may be that in which the wind speed is exceeded for 50% of the time. However if the purpose of the ventilation rate calculations is to determine overall winter heating requirements or extreme heat loss conditions for heating plant design it would be more appropriate to choose the conditions where the gradient wind speed is exceeded for 10% of the time and 1% of the time respectively.

Applying the data to the location of the low rise housing array described by example 1 in figure 15, situated in Sheffield, yields the following pressure drop values

$$\Delta C_{p1} = 0.104$$

(a) Odour Control Criteria

V_G (exceeded for 50% of time) = 9.4 m/s

$\frac{1}{2}\rho V_G^2 = 54.2 \ N/m^2$

$\therefore \ \Delta p = 5.6 \ N/m^2$

Hence Δpo the pressure drop acting across an infiltration aperture on either the windward or leeward faces is

$$\underline{\Delta po = 2.8 \ N/m^2}$$

(b) Winter Heating Criteria

V_G (exceeded for 10% of time) = 18.7 m/s

$\frac{1}{2}\rho V_G^2 = 214.4 \ N/m^2$

$\therefore \ \Delta p = 22.3 \ N/m^2$

Hence, $\underline{\Delta po = 11.15 \ N/m^2}$

(c) Extreme Heat Loss Criteria

V_G (exceeded for 1% of time) = 27.1 m/s

$\frac{1}{2}\rho V_G^2 = 450.2 \ N/m^2$

$\therefore \ \Delta p = 46.8 \ N/m^2$

Hence, $\underline{\Delta po = 23.4 \ N/m^2}$

The corresponding values of the roof leakage aperture pressure drop, Δpr, may be determined in a similar manner using figure 16 and Appendix A for the prediction of the pressure drop coefficient, together with Appendix B for the appropriate value of the gradient wind speed.

6. CONCLUSIONS

A prediction technique has been presented which enables the surface pressures acting on a particular building, situated within an array of similar low rise buildings, to be estimated. The procedure takes account of both the geometrical form of the building and the spacing parameters which describe the array as well as the direction of the wind and the upstream fetch conditions. The estimated value in the form of a pressure coefficient, non dimensionalised with respect to a gradient wind speed, may be determined by means of a graphical method. Data for the variation of the gradient wind speed over the United Kingdom, for three occurrence probability conditions, is presented in order that pressure drop values may be derived, subject to certain restrictions on the choice of site.

References

ASHRAE. (1972) Handbook of Fundamentals, American Society of Heating, Refrigeration and Air Conditioning Engineers. New York.

Bilsborrow, R.E. (1973) Natural Ventilation of Buildings. Ph.D. Thesis, University of Sheffield.

B.S.I. (1972) British Standards Institute, Code of Practice CP3, Wind Loads, London.

Counihan, J. (1973) Simulation of an Adiabatic Urban Boundary Layer in a Wind Tunnel. Jnl.Atmos.Envir., Vol. 7.

Dick, J. (1949) Experimental Studies in the Natural Ventilation of Houses. Jnl.Inst. Heating and Vent. Eng., Vol. 17.

E.S.D.U. (1971) Fluid Forces, Pressures and Moments on Rectangular Blocks. Engineering Societies Data Unit, Data Item 71016.

Good, M.C. and Joubert, P.N. (1968) The Form Drag of Two-Dimensional Bluff Plates Immersed in Turbulent Boundary Layers. Jnl. Fl. Mech. Vol. 31.

Hussain, M. (1979) A Study of the Wind Forces on Low Rise Building Arrays. Ph.D. Thesis, University of Sheffield.

I.H.V.E. (1970) Air Infiltration. Section A4. Institution of Heating and Ventilation Eng. Guide Book A. London.

Jackman, P.J. (1969) A Study of the Natural Ventilation of Tall Office Buildings. H.V.R.A. Laboratory Report No. 53.

Jensen, M. and Franck, N. (1965) Model Scale Tests in Turbulent Wind. Danish Tech. Press, Copenhagen.

Joubert, P.N., Perry A.E. and Stevens L.K. (1971) Drag of a Bluff Body Immersed in a Rough Wall Boundary Layer. Proc. 3rd Int. Conf. Wind Effects on Buildings and Structures. Tokyo.

Lee, B.E. (1978) The Simulation of Atmospheric Boundary Layers in the Sheffield University 1.2 x 1.2 m Boundary Layer Wind Tunnel. Proc. 3rd Coll. Ind. Aero., Fachhochschule Aachen, F.D.R., June.

Lee, B.E. and Soliman, B.F. (1977) — An Investigation of the Forces on Three Dimensional Bluff Bodies in Rough Wall Turbulent Boundary Layers. Trans A.S.M.E., Jnl. Fl. Engng., Vol. 99, Sept.

Morris, H.M. (1955) — Flow in Rough Conduits. Proc. A.S.C.E., Vol. 120, Paper 2745.

Newberry, C. and Eaton K. (1974) — The Wind Loading Handbook. Building Research Establishment Report, H.M.S.O.

Perry, A.E., Schofield, W.H. and Joubert, P.N. (1969) — Rough Wall Turbulent Boundary Layers. Jnl. Fl. Mech., Vol. 37, Pt.2.

Soliman, B.F. (1976) — A Study of the Wind Pressure Forces Acting on Groups of Buildings. Ph.D. Thesis, University of Sheffield.

Soliman, B.F. and Lee, B.E. (1974) — Some Aspects of Density and Form Relevant to Air Flow in Urban Areas. Build. International, Vol. 7.

Tielman, H.W. and Reinhold, T.A. (1976) — A Wind Tunnel Model Investigation for Basic Building Geometries. Rep. No. VPI-E-76-8, Dept. of Engng. Sci. and Mech., Virginia Poly. Inst. and State Univ., Blacksburg, Va.

Wooding, R.A., Bradley, E.F. and Marshall, J.K. (1973) — Drag Due to Regular Arrays of Roughness Elements of Varying Geometry. Boundary Layer Met., Vol.5.

Appendix A

The Assessment of Internal Pressures

It is apparent from the discussion of roof pressure variations that a means of determining the building's internal pressure is required in order to quantify the infiltration which may take place via openings in the roof. The pressure difference term on which the roof infiltration rate depends then becomes

$$\Delta p_r = \Delta C_{pr} \cdot \tfrac{1}{2} \rho V_G^2$$

$$= (C_{s1} - C_{pir}) \cdot \tfrac{1}{2} \rho V_G^2$$

where C_{pir} is the internal pressure within the building, assuming that the external surface may have openings in all vertical walls and on the roof.

The method for predicting the internal pressure of a low rise building which forms part of an array of similar buildings has been based on the use of external surface pressure coefficient measurements determined by the procedure described in section 3. The method of analysis follows that described by Newberry and Eaton (1974).

The quantity of air Q, flowing through any aperture is proportional to the cross-sectional area, A, of the aperture and, to a first approximation, to the square root of the pressure drop $(p_e - p_i)$ across it. Since the volume of air entering the building must equal the volume of air leaving the building, the summation of Q at all leakage points must be zero.

Thus:

$$\Sigma A (p_e - p_i)^{\frac{1}{2}} = 0$$

$$\text{or} \quad \Sigma A (C_{pe} - C_{pi})^{\frac{1}{2}} = 0 \qquad \text{Eqn. A1}$$

If we assume initially that leakage apertures exist only on the windward face of a building, aperture area Aw, and the sides and rear of the building, aperture area Ab, whose surfaces are under suction, equation A1 can be written as follows.

$$A_w(C_{pw} - C_{pis})^{\frac{1}{2}} + A_b(C_{pb} - C_{pis})^{\frac{1}{2}} = 0$$

from which it follows that

$$C_{pis} = \frac{(Aw/Ab)^2 C_{pw} + C_{pb}}{1 + (Aw/Ab)^2} \qquad \text{Eqn. A2}$$

Hence equation A2 enables the internal pressure coefficient, dependent only on apertures on the vertical walls of a building, to be expressed in terms of the ratio of the relevant open areas under suction and pressure and the external surface pressure coefficients themselves.

The major part of the paper has demonstrated that the external surface pressure coefficients are functions of both the geometrical form of the building and the form of the group in which the building is situated, and thus the internal pressure coefficient will be similarly dependent on these parameters. Using equation A2, figures A1 to A8 have been produced for each of the building shapes considered, identified by a pair of values of A_f and A_s, the frontal and side aspect ratios of the building respectively. In these figures the internal pressure coefficient, C_{pis}, is plotted against the aperture area ratio Aw/Ab, which is shown over the range 0.1 to 10.0. In order to include the dependence of pressure forces on group form each of the graphs for a particular building shape has been plotted for five values of the group clear spacing ratio Sc/H from 1.0 to 5.0, thus covering the range of practical application. These graphs then enable the internal pressure coefficient to be obtained quite simply for the cases where no air leakage apertures occur in the roof. For the examples indicated on figure 15, the value of C_{pis} for Example 1 may be found from graph A.3 as 0.034 for a leakage area ratio Aw/Ab equal to unity.

Similarly, Example 2 on figure 15 has a value of C_{pis} of 0.020 for the same leakage area ratio, see graph A.6.

If it is now assumed that leakage apertures exist in the roof in addition to the vertical walls, equation A1 can be written

$$A_w(C_{pw}-C_{pir})^{\frac{1}{2}} + A_b(C_{pb}-C_{pir})^{\frac{1}{2}} + Ar(C_{s1}-C_{pir})^{\frac{1}{2}} = 0$$

i.e. $$C_{pir}\left\{1 + \left(\frac{Aw}{Ab}\right)^2 + \left(\frac{Ar}{Ab}\right)^2\right\} = \left(\frac{Aw}{Ab}\right)^2 C_{pw} + C_{pb} + \left(\frac{Ar}{Ab}\right)^2 C_{s1}$$

hence $$C_{pir} = \frac{C_{pis}\left\{1+(Aw/Ab)^2\right\} + (Ar/Ab)^2\, Cs1}{\left\{1 + (Aw/Ab)^2 + (Ar/Ab)^2\right\}} \qquad \text{Eqn. A3}$$

Equation A3 then enables the internal pressure coefficient C_{pir} to be determined from other known data. In order to illustrate this procedure Example 1 from figure 16 is used, where a value of C_{s1} of −0.074 is found for the building form and group form variables chosen. If Aw/Ab is assumed to be 1.0 then the appropriate value of C_{pis} from figure A.5 is found to be 0.028 and hence C_{pir} can be determined for any value of Ar/Ab. If a value of Ar/Ab of 0.10 is assumed C_{pir} becomes

$$C_{pir} = \frac{.028\{1 + 1\} + (-.74)(.01)}{\{1 + 1 + .01\}}$$

i.e. $C_{pir} = .0242$

Hence the value of ΔC_{pr} to be used in the infiltration rate equation becomes

$$\Delta C_{pr} = \left(C_{s1} - C_{pir}\right)$$
$$= -.074 - .024$$
$$= \underline{-.098}$$

The negative sign indicates that the direction of the roof infiltration flow is from the interior of the building to the exterior.

Details of how this simplified approach to the determination of internal pressures may be extended to the problems of buildings with multiple internal divisions are outlined by Newberry and Eaton (1974).

Appendix B

Gradient Wind Speeds Over the United Kingdom

Throughout this paper reference has been made to pressure coefficients formed by normalising pressures with respect to a dynamic head based on the wind tunnel free stream velocity, i.e. that velocity at the top of the modelled boundary layer. The full scale analogue of this free stream velocity is known as the gradient velocity, whose value is determined by the global atmospheric pressure distribution and by the forces on air particles which arise as a consequence of the rotation of the earth.

Thus in order to obtain the pressure difference acting on a real building at a particular location it is necessary to multiply the appropriate pressure difference coefficient found from the prediction procedure by the dynamic head based on the full scale gradient wind speed. Such data for the United Kingdom is relatively scarce but that contained in Caton (1975) is sufficient for the present purpose. Figures B1, B2 and B3 show the distribution of gradient wind speeds (speeds at 900 m elevation) over the United Kingdom for 3 conditions, these conditions being speeds exceeded for 50%, 10% and 1% of the time, i.e. 4380 hours, 876 hours and 88 hours per annum respectively. The choice of time period, discussed in the paper, will be dependent on the use to which the ventilation rate data are to be applied.

The values of the gradient wind speed may be used directly in the calculation of the design values of the pressure difference without application of correction factors. The influence of building height is negligible provided that it is very small compared with the boundary layer height. In the case of the present model experiments this ratio has the value 0.045 and in a typical full scale case, of 10 m high buildings in a boundary layer 500 m deep, would have a value of 0.020. Hence this method is only applicable to low rise building arrays where the individual buildings are of one, two or three storeys high, and are thus in a height range where no reliable general rules exist for the prediction of full scale wind speeds.

The influence of upstream terrain has already been included in the prediction procedure for the pressure coefficient values by virtue of the experimental method itself, utilising a simulated suburban atmospheric flow, and so no terrain velocity correction factor is required.

However, it is important to realise that the full scale analogy of this modelling procedure will necessarily restrict the application of the prediction technique to those areas of the United Kingdom where the chosen boundary layer characteristics are appropriate. Hence the technique will be applicable to suburban areas on approximately level ground

at inland sites. It will not apply to sites in coastal regions or to mountainous areas, where ground level wind drag conditions are dissimilar to those implied by the modelling analogue, and hence have different vertical wind speed gradients.

It is interesting to note that although the model building arrays have been tested in a suburban atmospheric boundary layer simulation, this particular incident flow will only influence values of the pressure coefficients for building arrays in the isolated roughness flow regime. For arrays in both the wake interference and skimming flow regimes, where the fetch length is sufficient for flow stabilisation, ($R/H > 25$), the surface pressures depend only on the flow in the internal boundary layer which grows over the array layout itself and so are effectively independent of the nature of the incident flow. Thus the results for these two flow regimes are more widely applicable than the restrictions of the test programme imply, subject to the limitations on the overall location of the site discussed in the previous paragraph.

This appendix on the choice of a gradient wind speed is considered by the authors only as a tentative guide. The choice of an appropriate gradient wind speed for any site location in the United Kingdom is a subject which perhaps warrants further discussion.

List of Figures

Appendix A

Figure A.1 The Variation of Internal Pressure Coefficient, Cpis with Aperture Ratio, Aw/Ab for $A_f = 0.5$, $A_s = 1.0$.

Figure A.2 The Variation of Internal Pressure Coefficient, Cpis, with Aperture Ratio, Aw/Ab, for $A_f = 1.0$, $A_s = 1.0$.

Figure A.3 The Variation of Internal Pressure Coefficient, Cpis, with Aperture Ratio, Aw/Ab for $A_f = 1.5$, $A_s = 1.0$.

Figure A.4 The Variation of Internal Pressure Coefficient, Cpis, with Aperture Ratio, Aw/Ab for $A_f = 2.0$, $A_s = 1.0$.

Figure A.5 The Variation of Internal Pressure Coefficient, Cpis, with Aperture Ratio, Aw/Ab for $A_f = 4.0$, $A_s = 1.0$.

Figure A.6 The Variation of Internal Pressure Coefficient, Cpis, with Aperture Ratio, Aw/Ab for $A_f = 1.0$, $A_s = 0.5$.

Figure A.7 The Variation of Internal Pressure Coefficient, Cpis, with Aperture Ratio, Aw/Ab for $A_f = 1.0$, $A_s = 1.5$.

Figure A.8 The Variation of Internal Pressure Coefficient, Cpis, with Aperture Ratio, Aw/Ab for $A_f = 1.0$, $A_s = 2.0$.

Appendix B

Figure B.1 Variation of Gradient Wind Speed over the United Kingdom. Speeds exceeded 50% of the time.

Figure B.2 Variation of Gradient Wind Speed over the United Kingdom. Speeds exceeded 10% of the time.

Figure B.3 Variation of Gradient Wind Speed over the United Kingdom. Speeds exceeded 1% of the time.

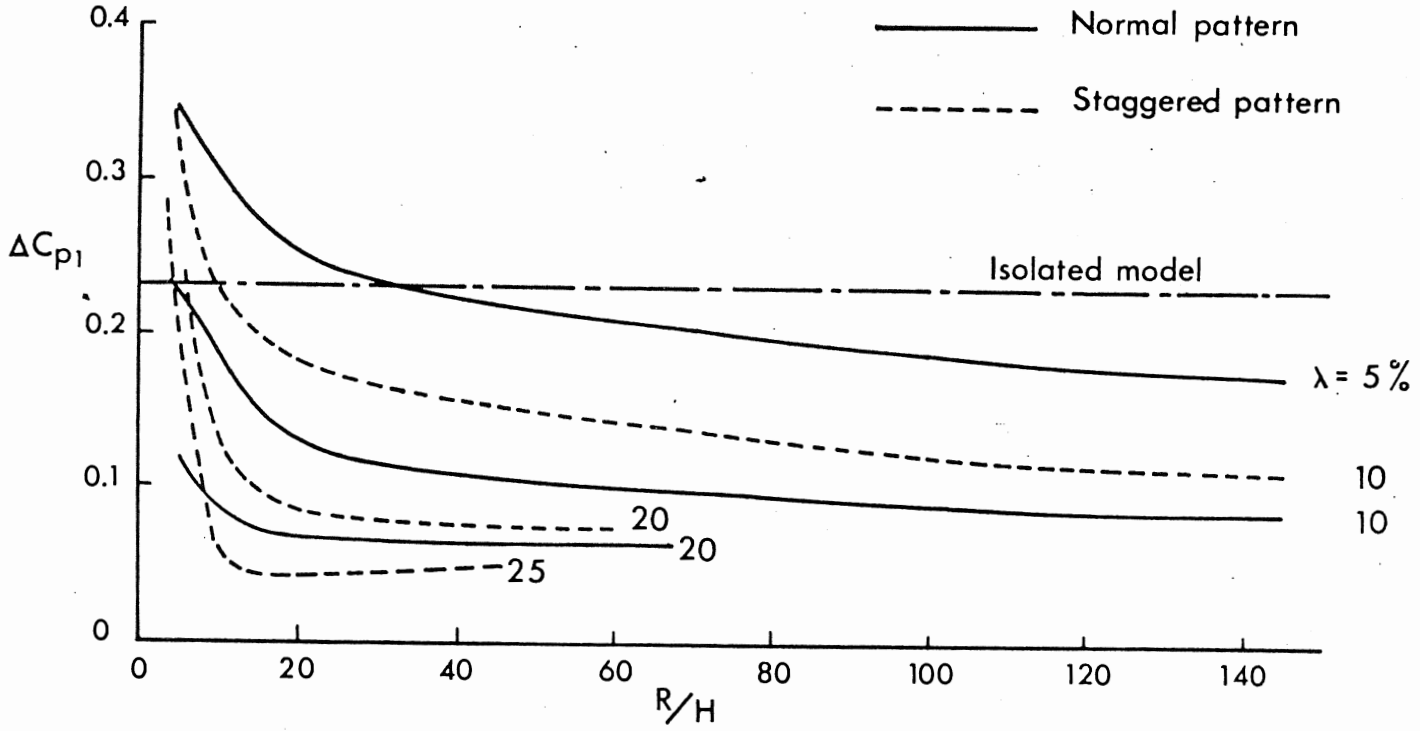

Figure 1 The Influence of Upstream Fetch Length on the Pressure Difference Coefficient. Cuboid Models.

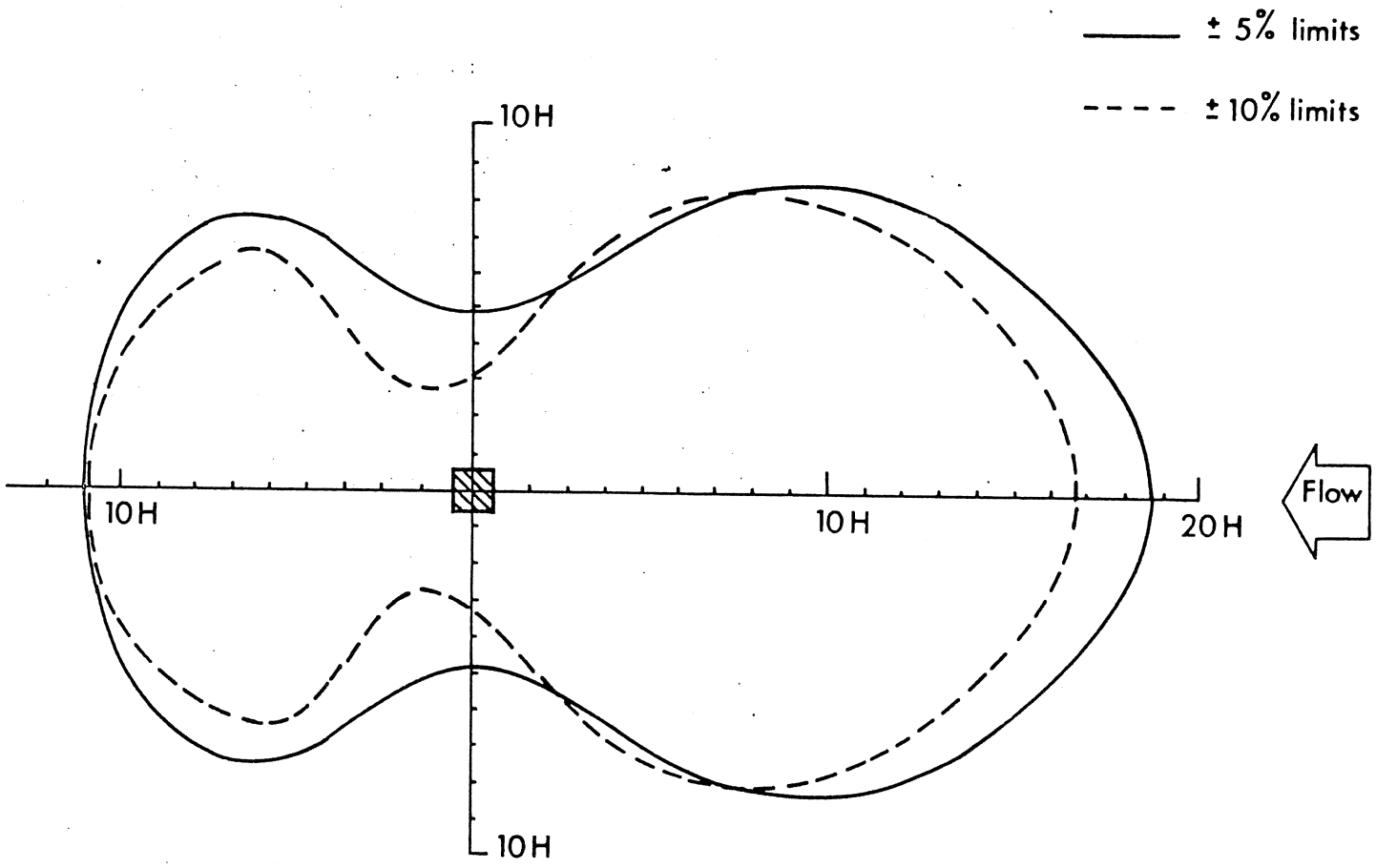

Figure 2 Limits of the Influence Area Around the Model. Cuboid Models. Normal Pattern. 10% Plan Area Density.

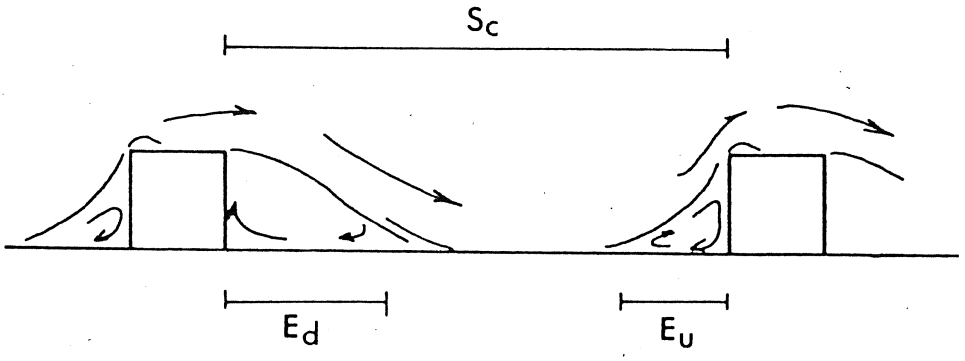

(a) Isolated Roughness Flow Regime

$S_c > E_t$

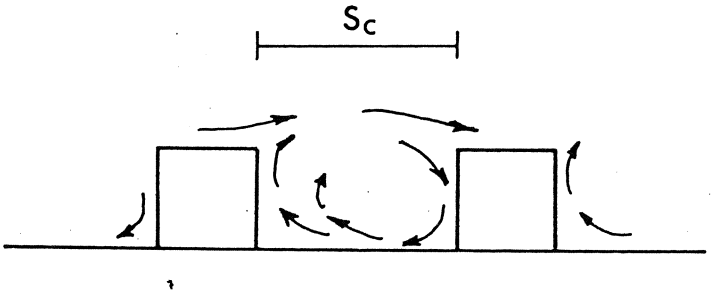

(b) Wake Interference Flow Regime

$E_v < S_c < E_t$

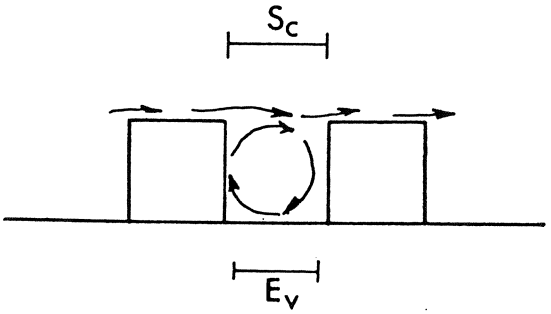

(c) Skimming Flow Regime

$S_c \leqslant E_v$

Figure 3 The Governing Conditions for the Three Flow Regimes.

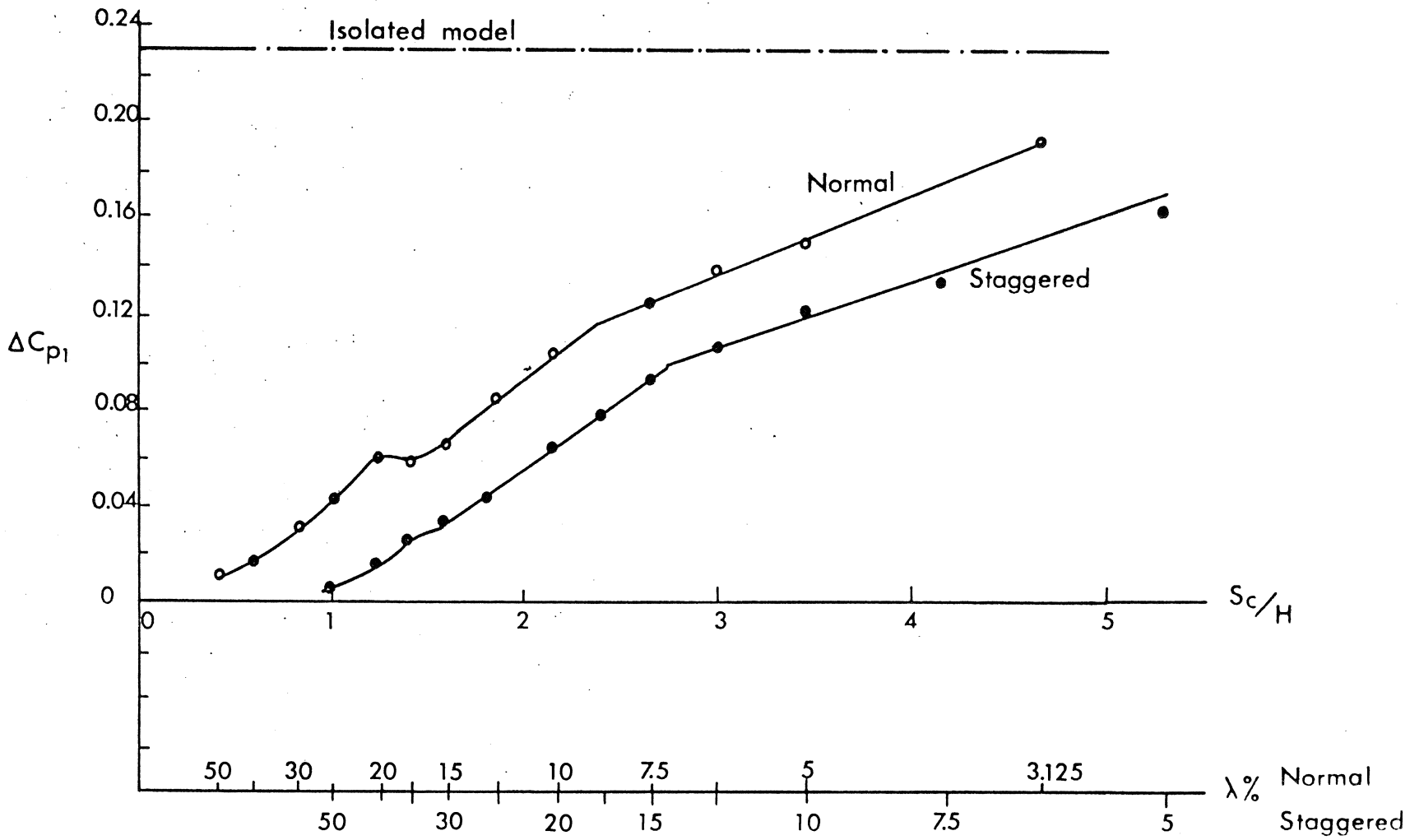

Figure 4 The Variation of Pressure Difference Coefficient with Array Spacing and Plan Area Density. Cuboid Models.

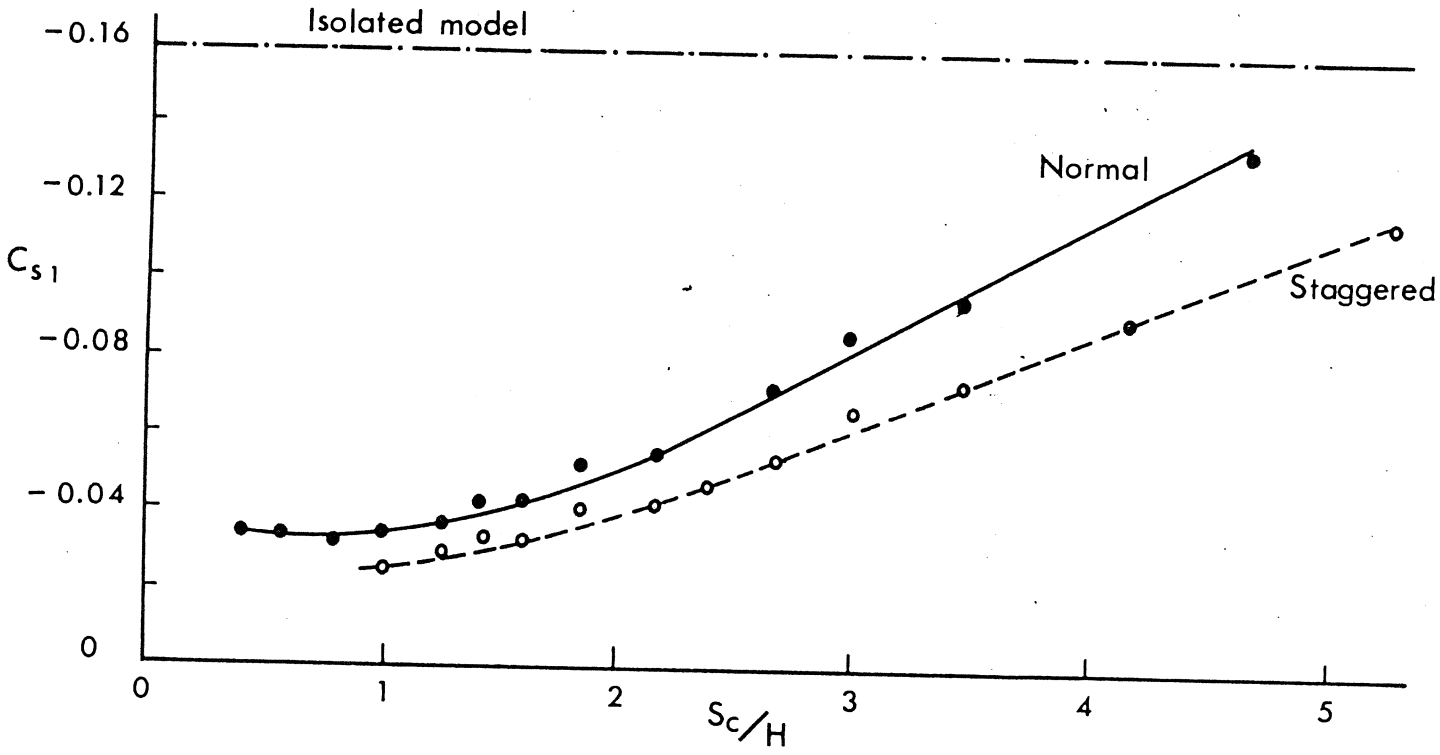

Figure 5 The Variation of Roof Suction Coefficient with Array Spacing. Cuboid Models.

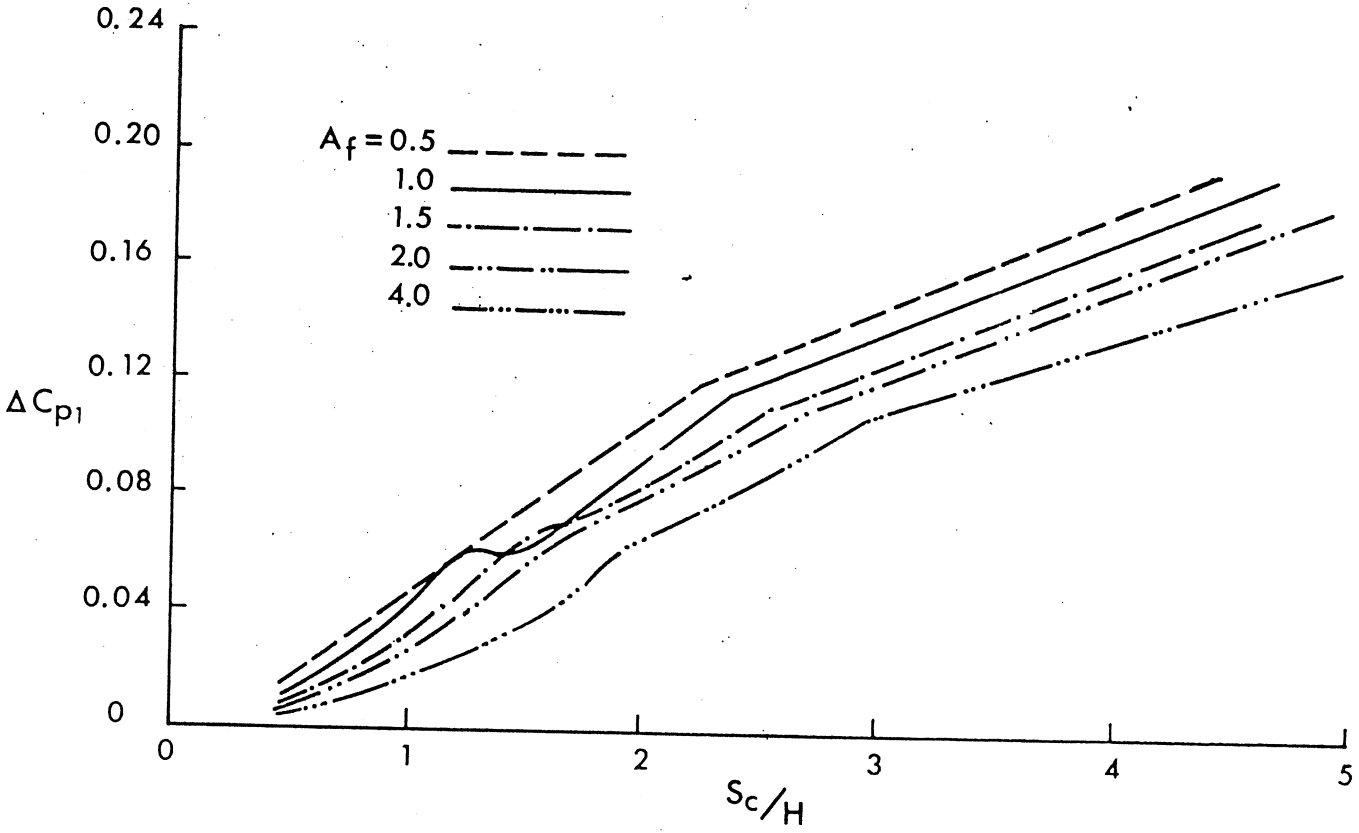

Figure 6 The Variation of Pressure Difference Coefficient with Array Spacing. Variable Frontal Aspect Ratio Models. Normal Pattern.

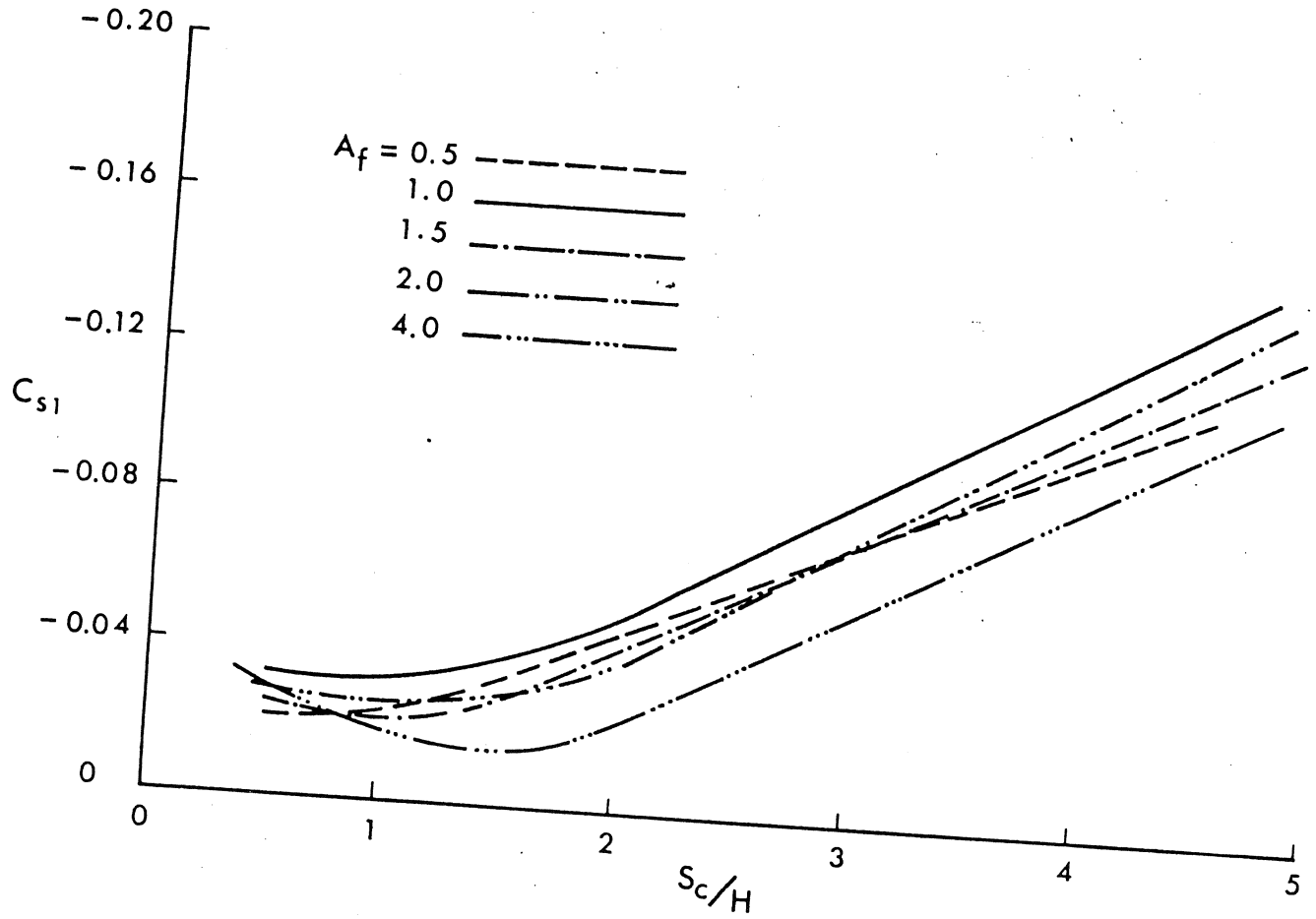

Figure 7 The Variation of Roof Suction Coefficient with Array Spacing. Variable Frontal Aspect Ratio Models. Normal Pattern.

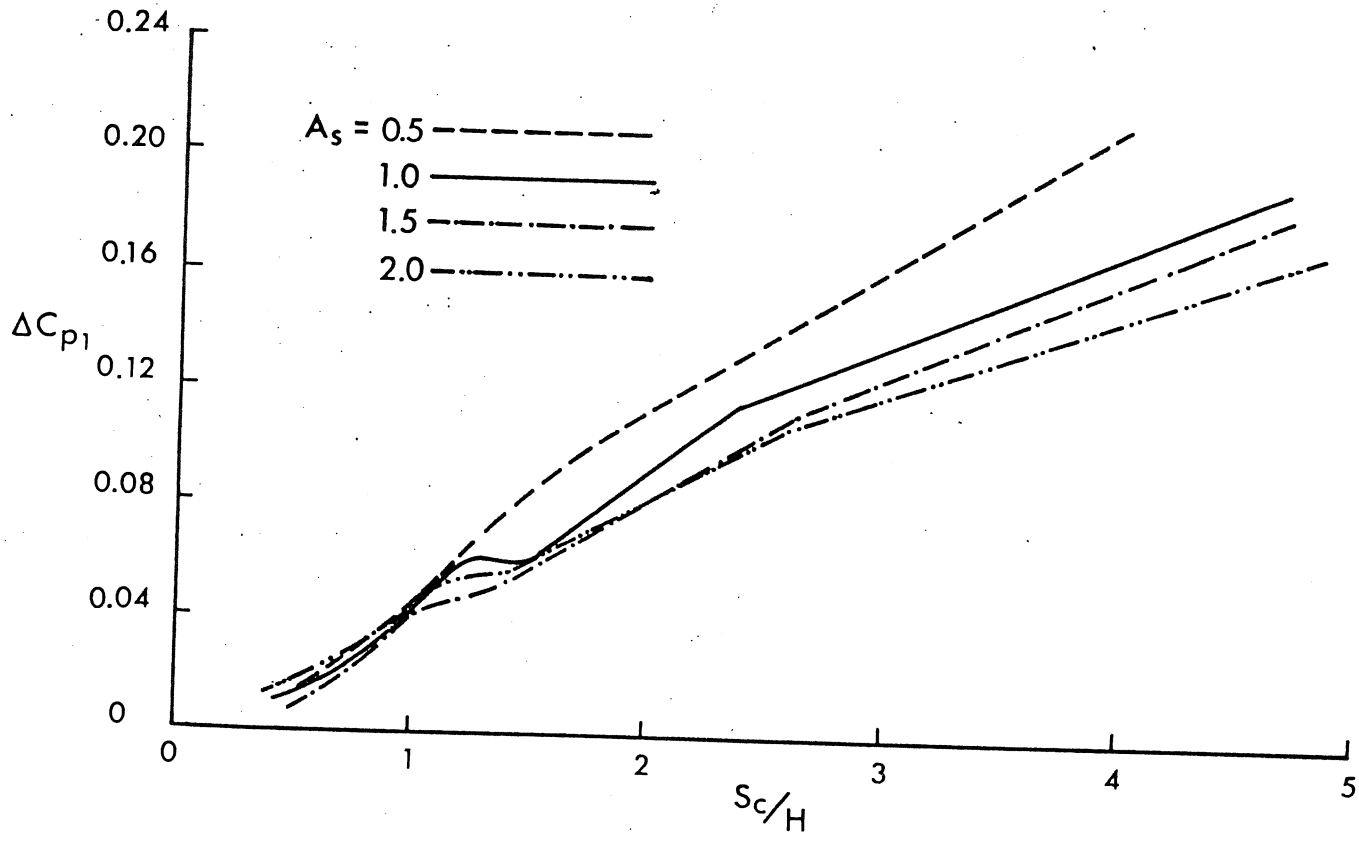

Figure 8 The Variation of Pressure Difference Coefficient with Array Spacing. Variable Side Aspect Ratio Models. Normal Pattern.

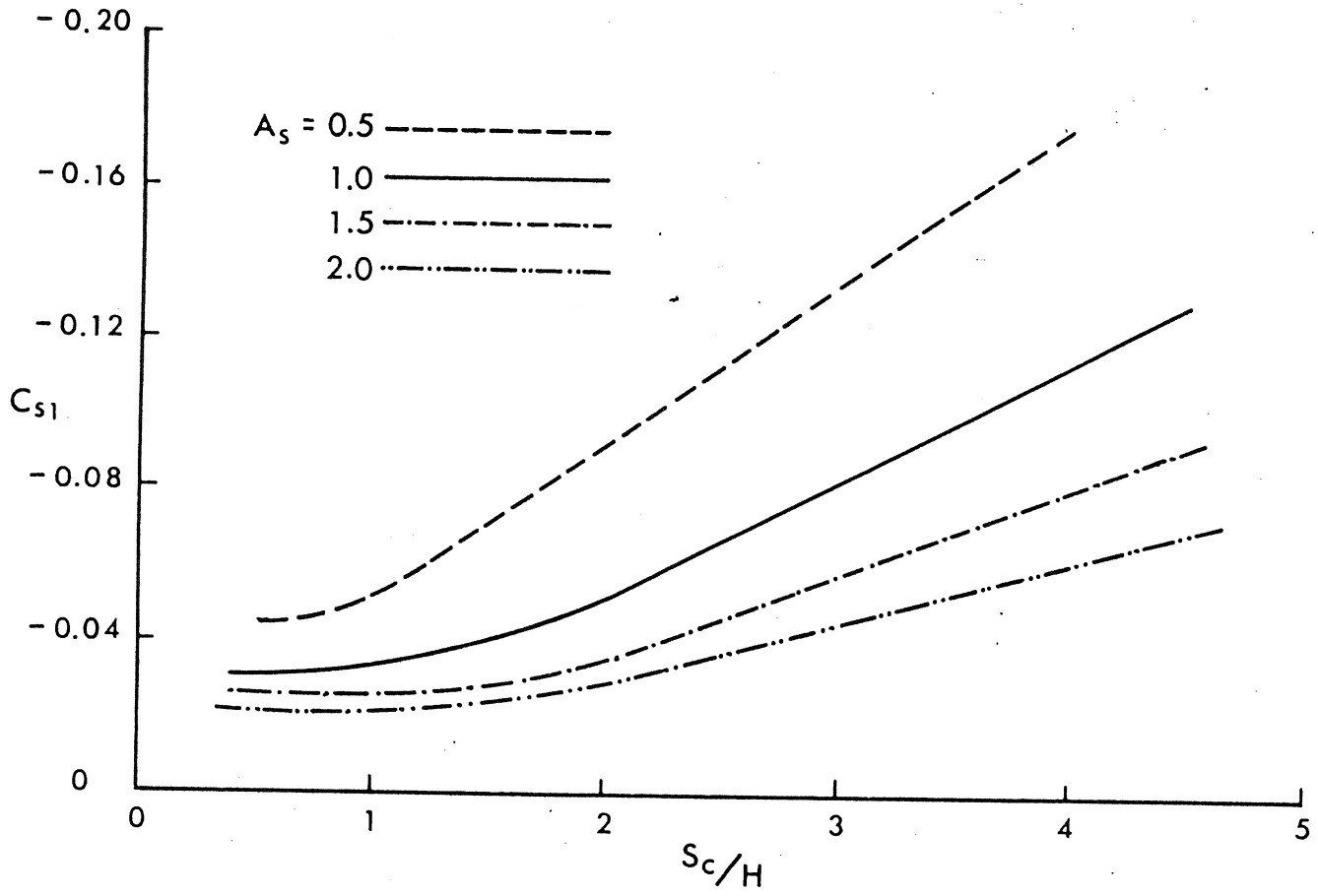

Figure 9 The Variation of Roof Suction Coefficient with Array Spacing. Variable Side Aspect Ratio Models. Normal Pattern.

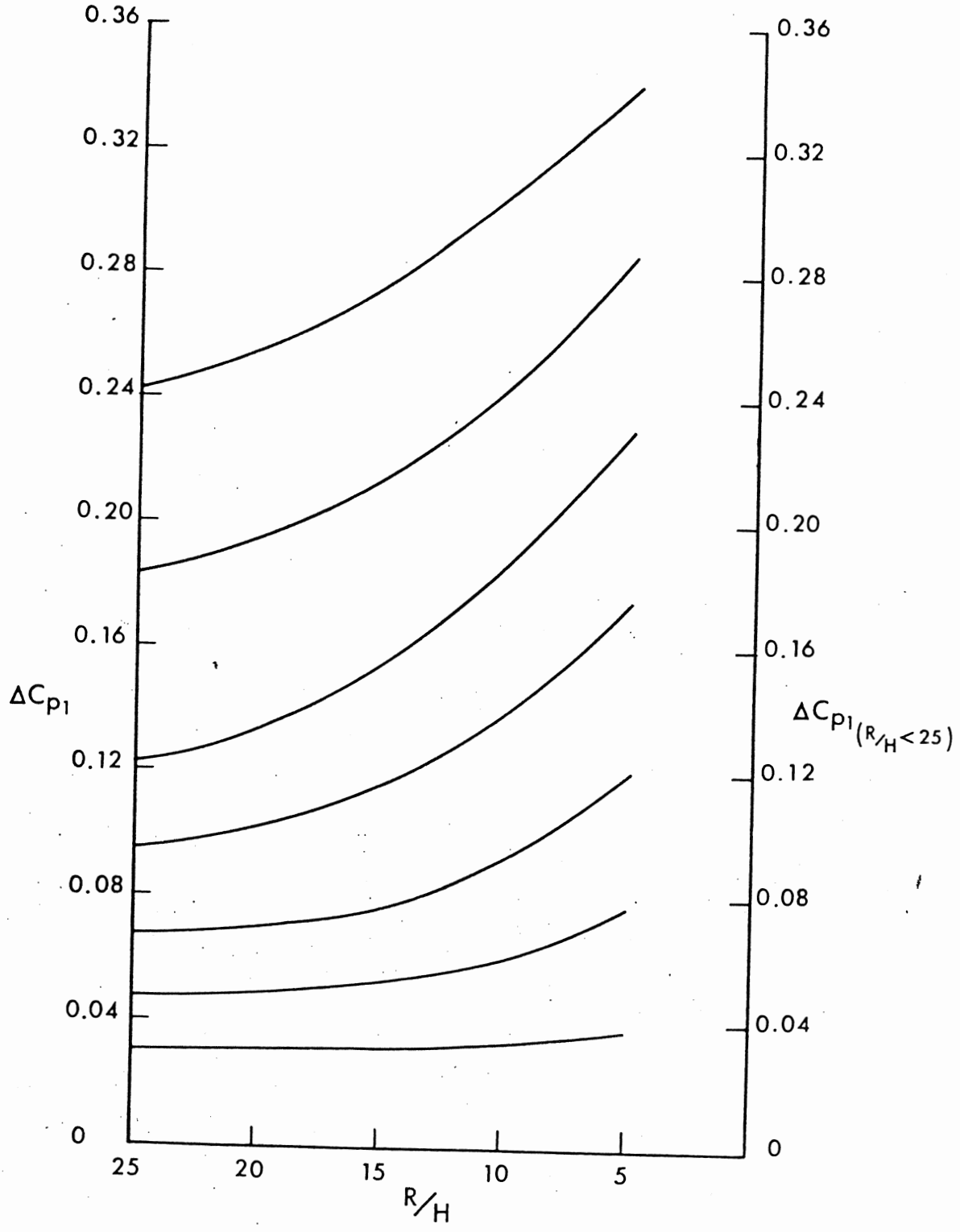

Figure 10 The Influence of Short Upstream Fetch Lengths on the Pressure Difference Coefficient.

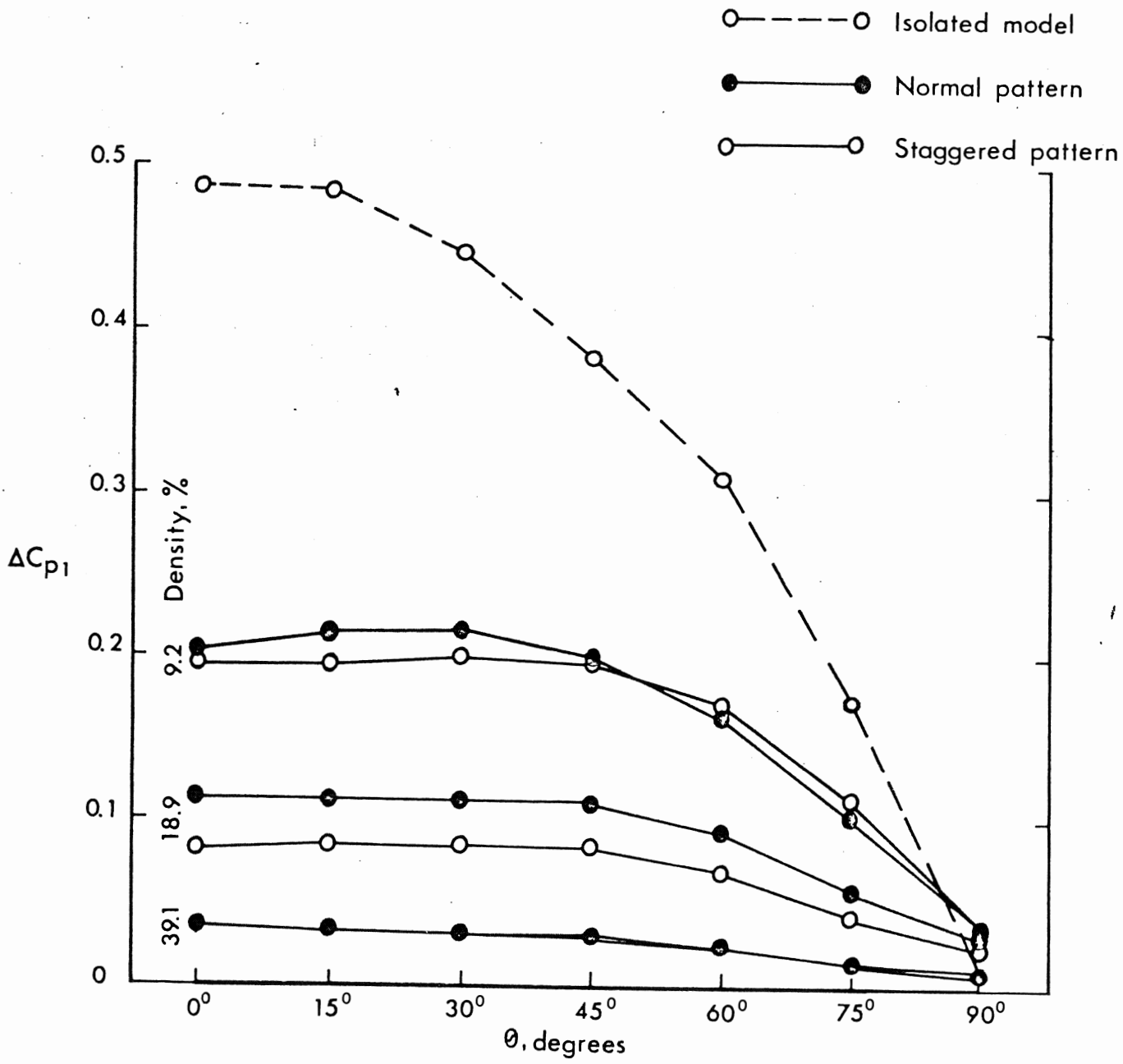

Figure 11 The Variation of Pressure Difference Coefficient with Wind Direction. Cuboid Models.

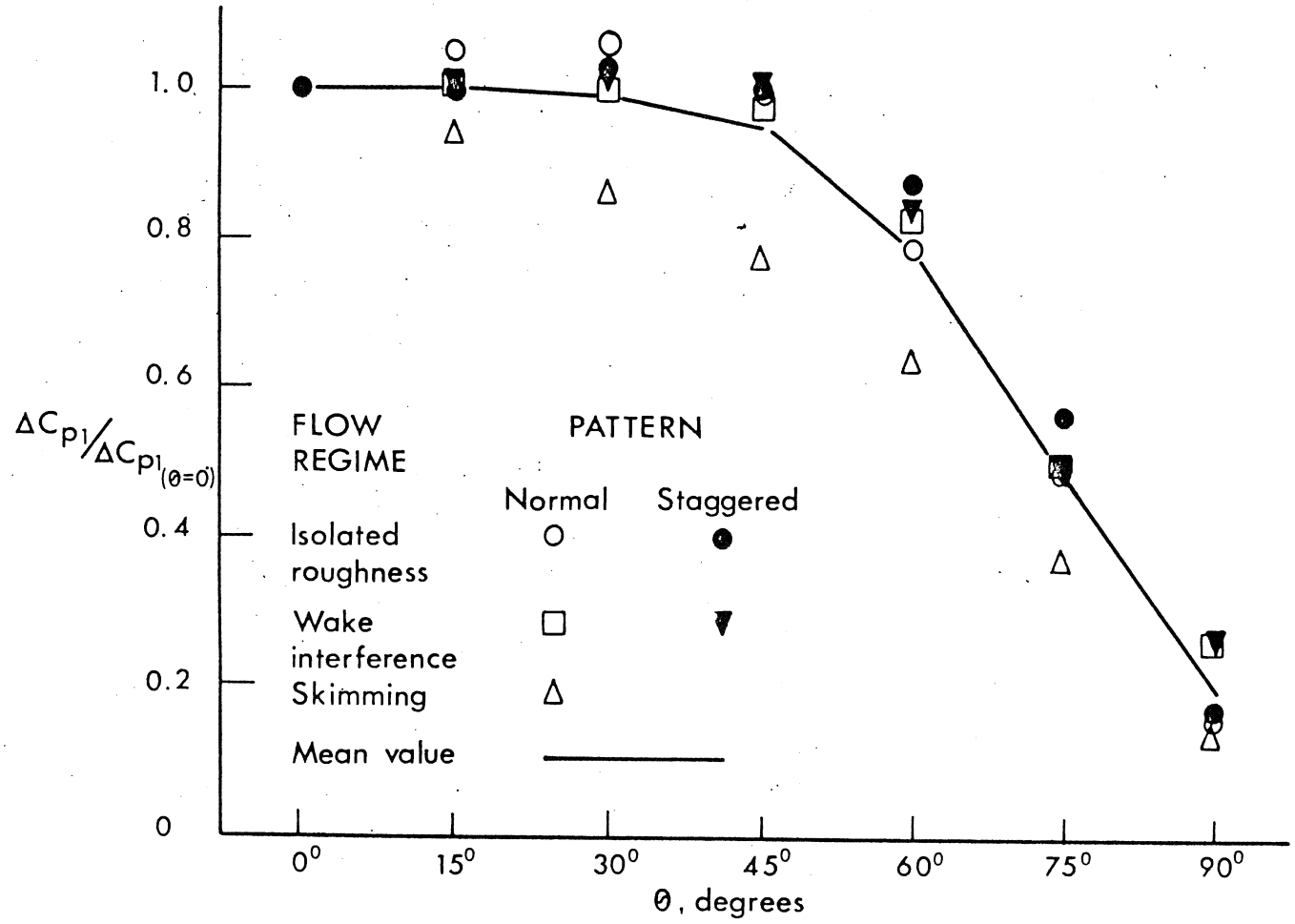

Figure 12 Variation of the Normalised Pressure Difference Coefficient with Wind Direction. Cuboid Models.

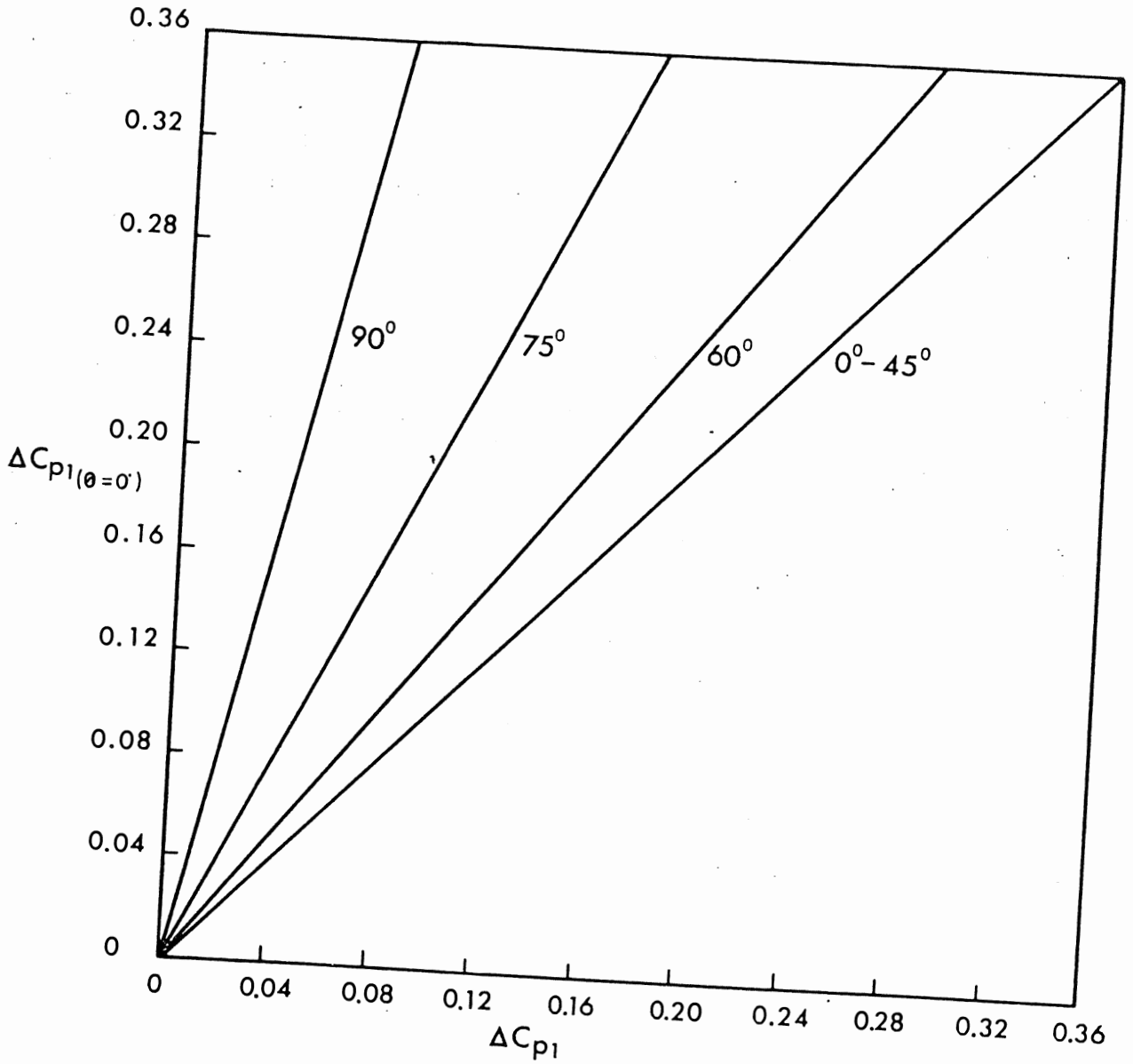

Figure 13 Wind Direction Correction for Pressure Difference Coefficients.

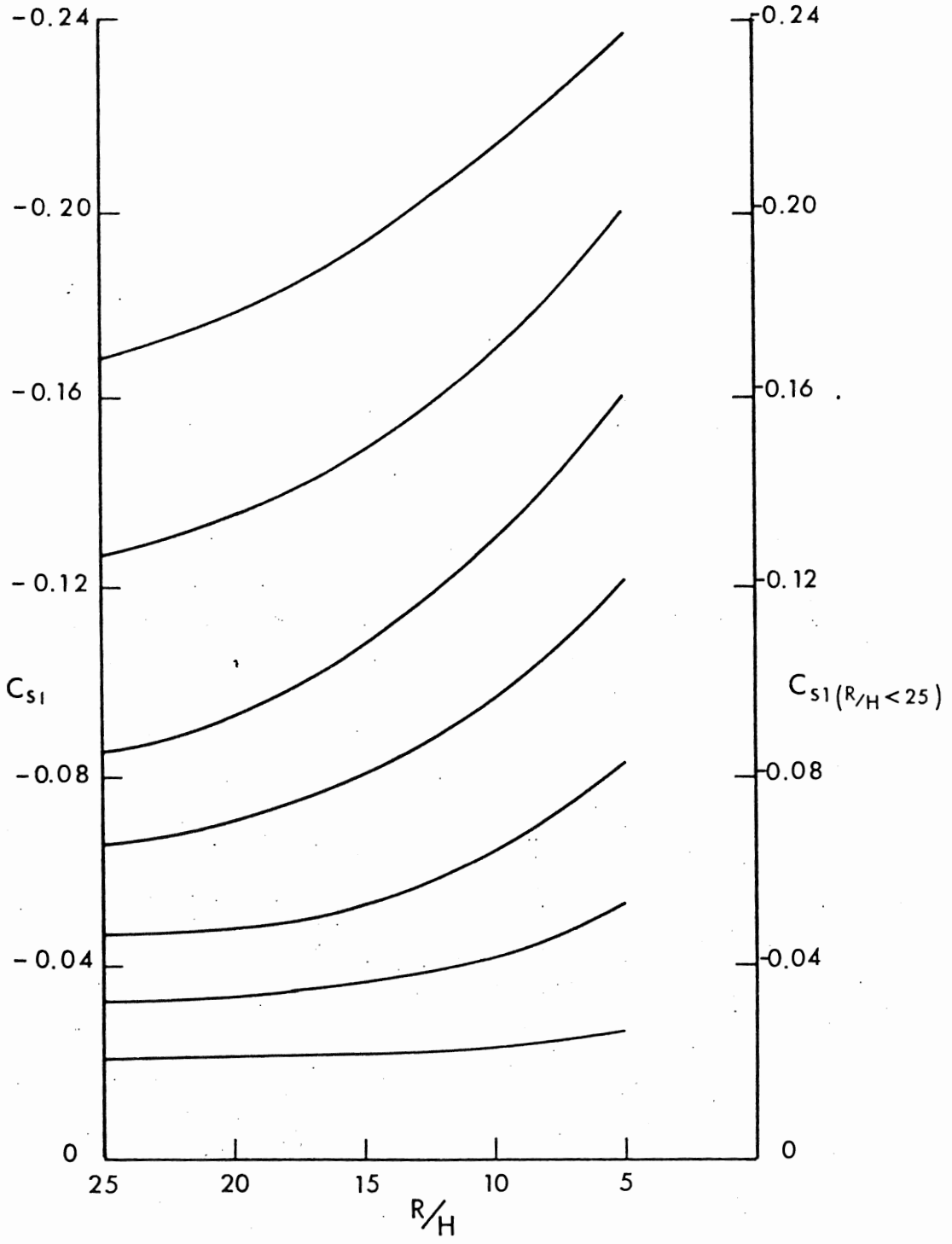

Figure 14 The Influence of Short Upstream Fetch Lengths on the Roof Suction Coefficients.

Example 1 : $A_f = 1.5$, $A_s = 1.0$, $S_c/H = 3.0$, $R/H > 25$, $\theta = 60^0$: $\Delta C_{p1} = 0.104$

Example 2 : $A_f = 1.0$, $A_s = 0.5$, $S_c/H = 3.5$, $R/H = 15$, $\theta = 0^0$: $\Delta C_{p1} = 0.228$

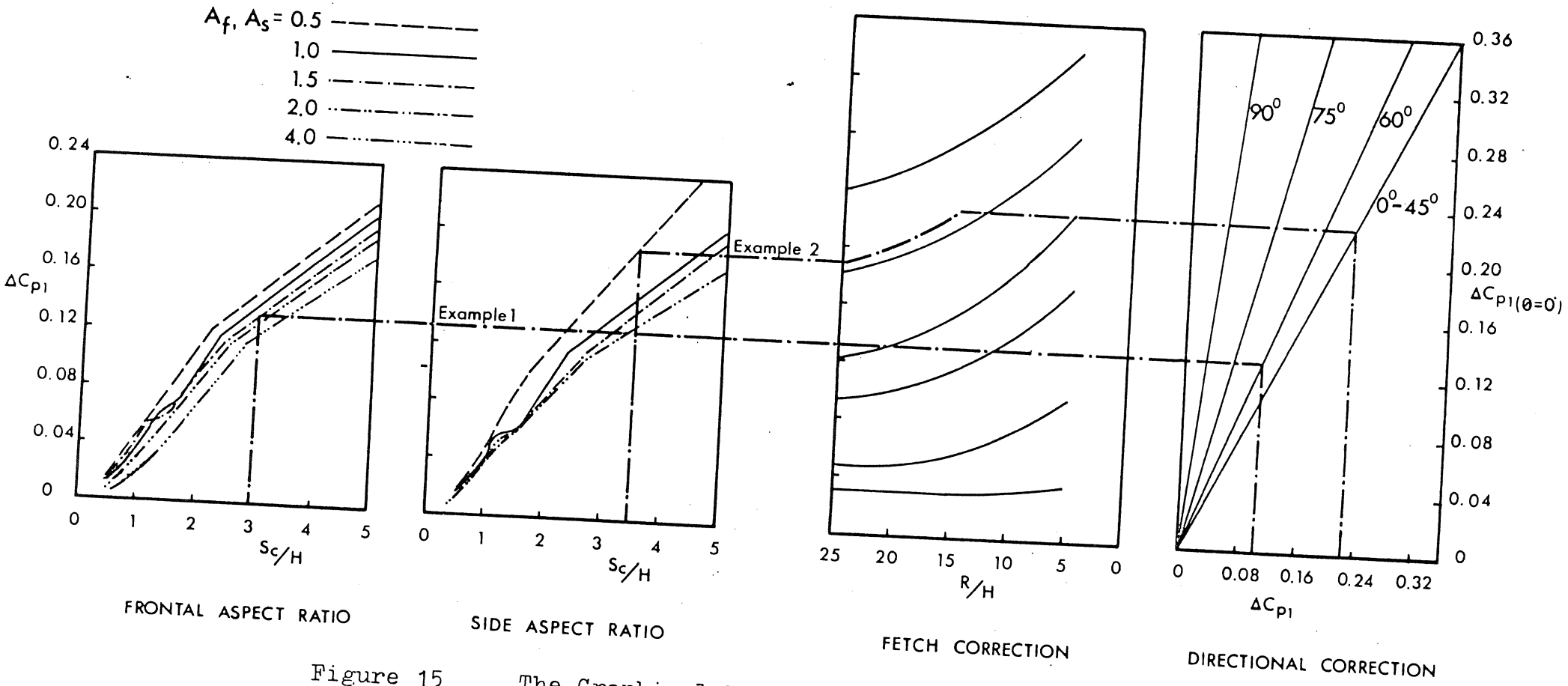

Figure 15 The Graphical Prediction Technique for Pressure Difference Coefficients.

Example 1 : $A_f = 4.0$, $A_s = 1.0$, $S_c/H = 3.5$, $R/H > 25$: $C_{s1} = -0.074$

Example 2 : $A_f = 1.0$, $A_s = 0.5$, $S_c/H = 2.0$, $R/H = 15$: $C_{s1} = -0.120$

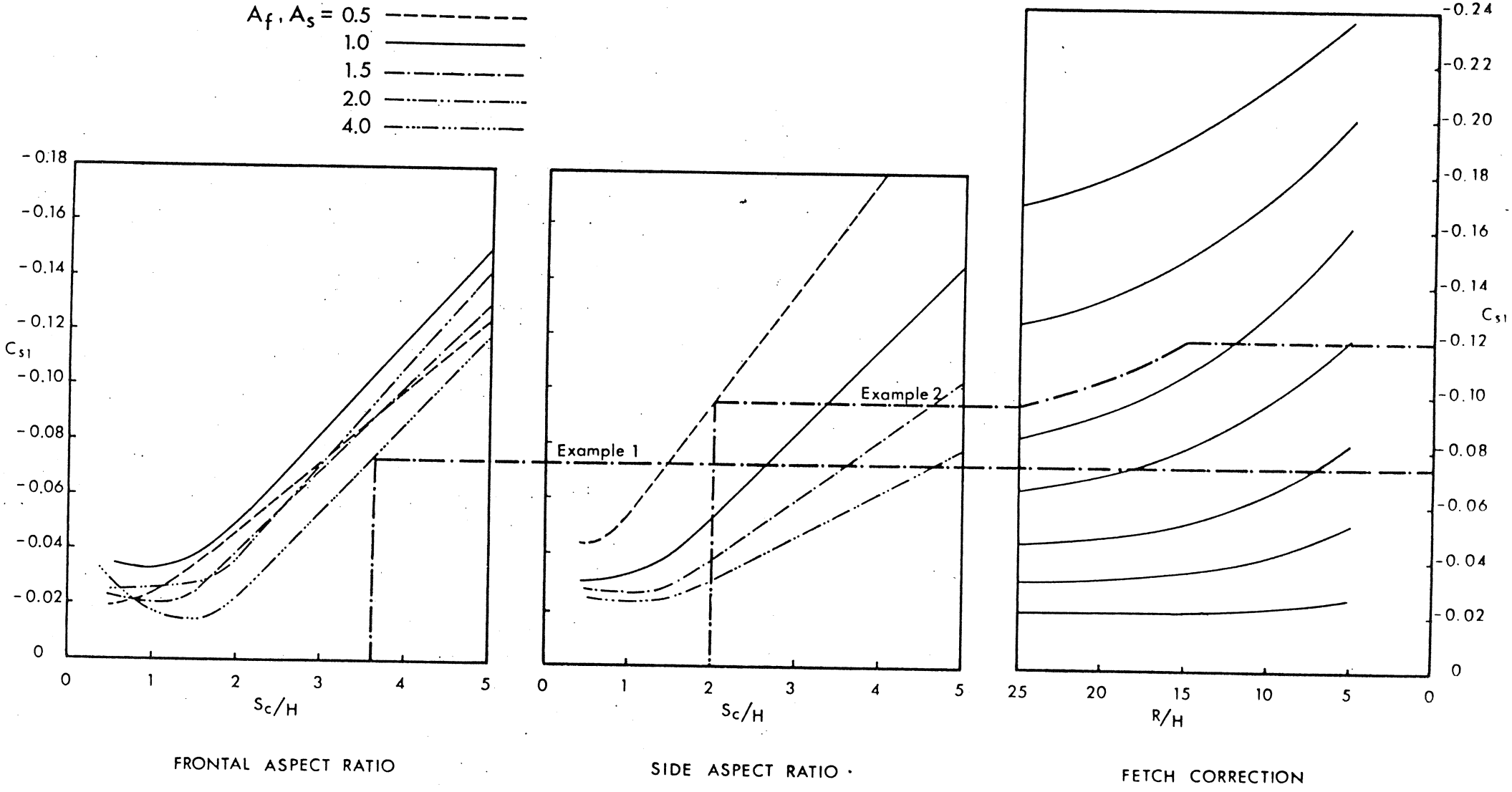

Figure 16 - The Graphical Prediction Technique for Roof Suction Coefficients.

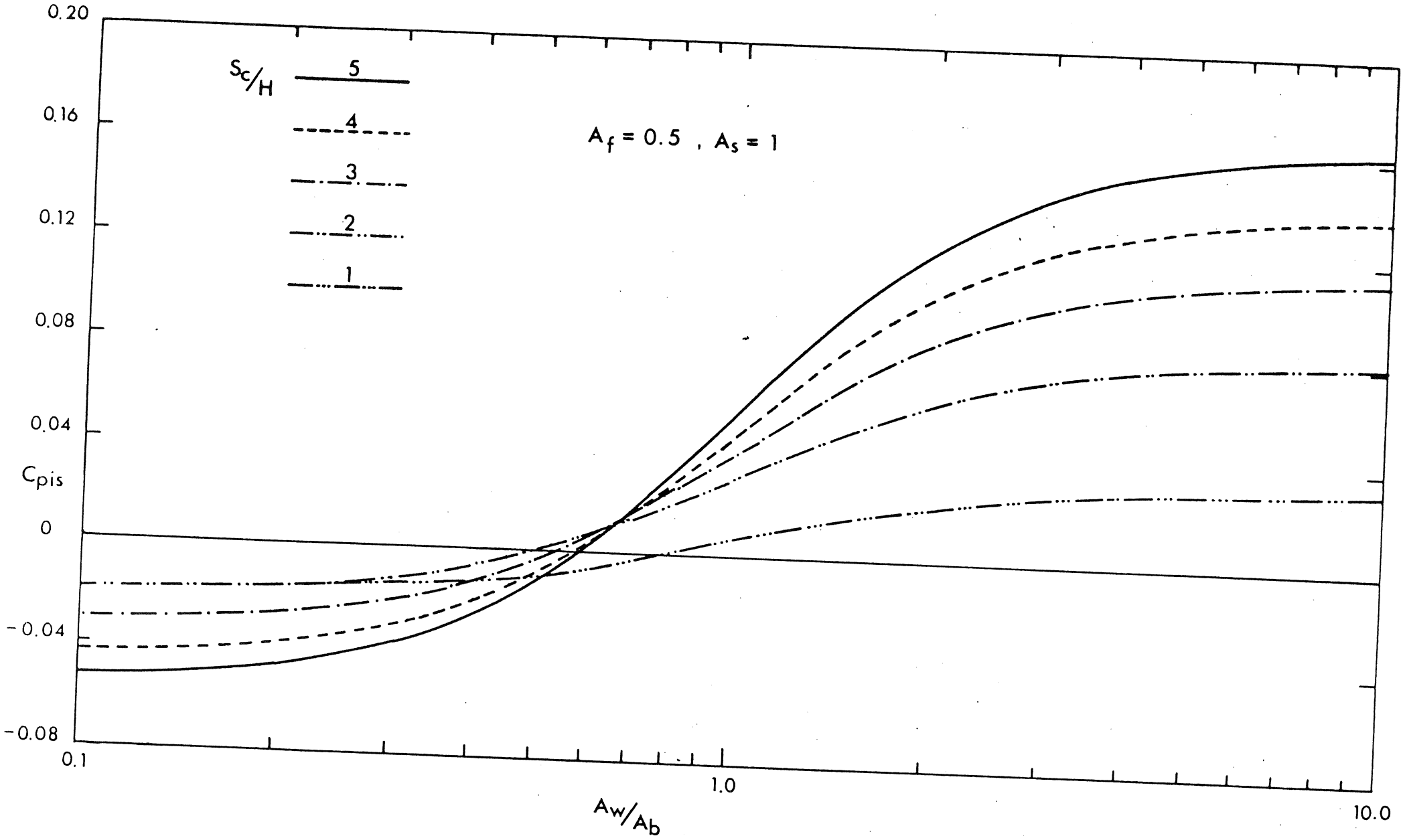

Figure A.1 The Variation of Internal Pressure Coefficient, Cpis, with Aperture Ratio, Aw/Ab for $A_f = 0.5$, $A_s = 1.0$.

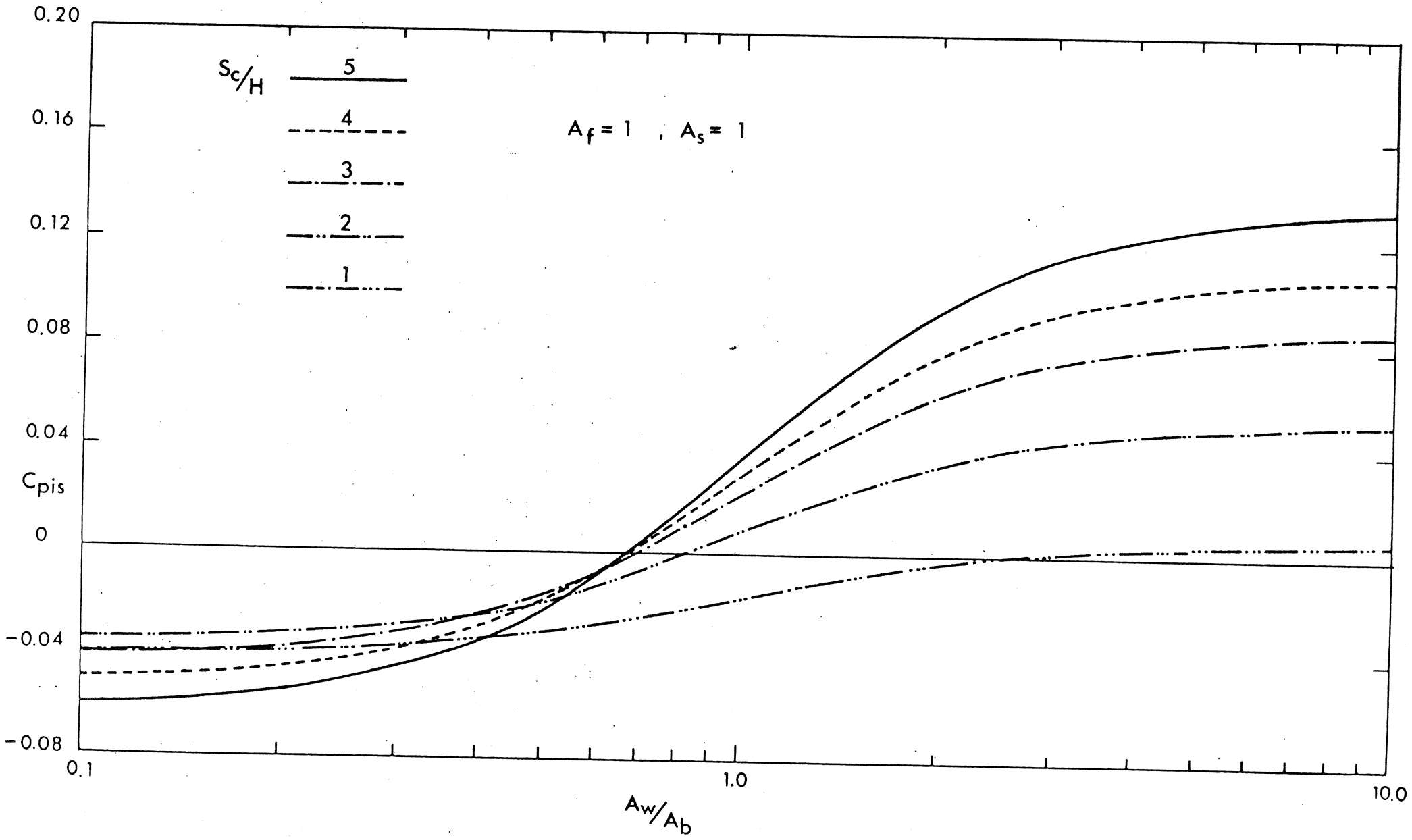

Figure A.2 The Variation of Internal Pressure Coefficient, Cpis, with Aperture Ratio, Aw/Ab for A_f = 1.0, A_s = 1.0.

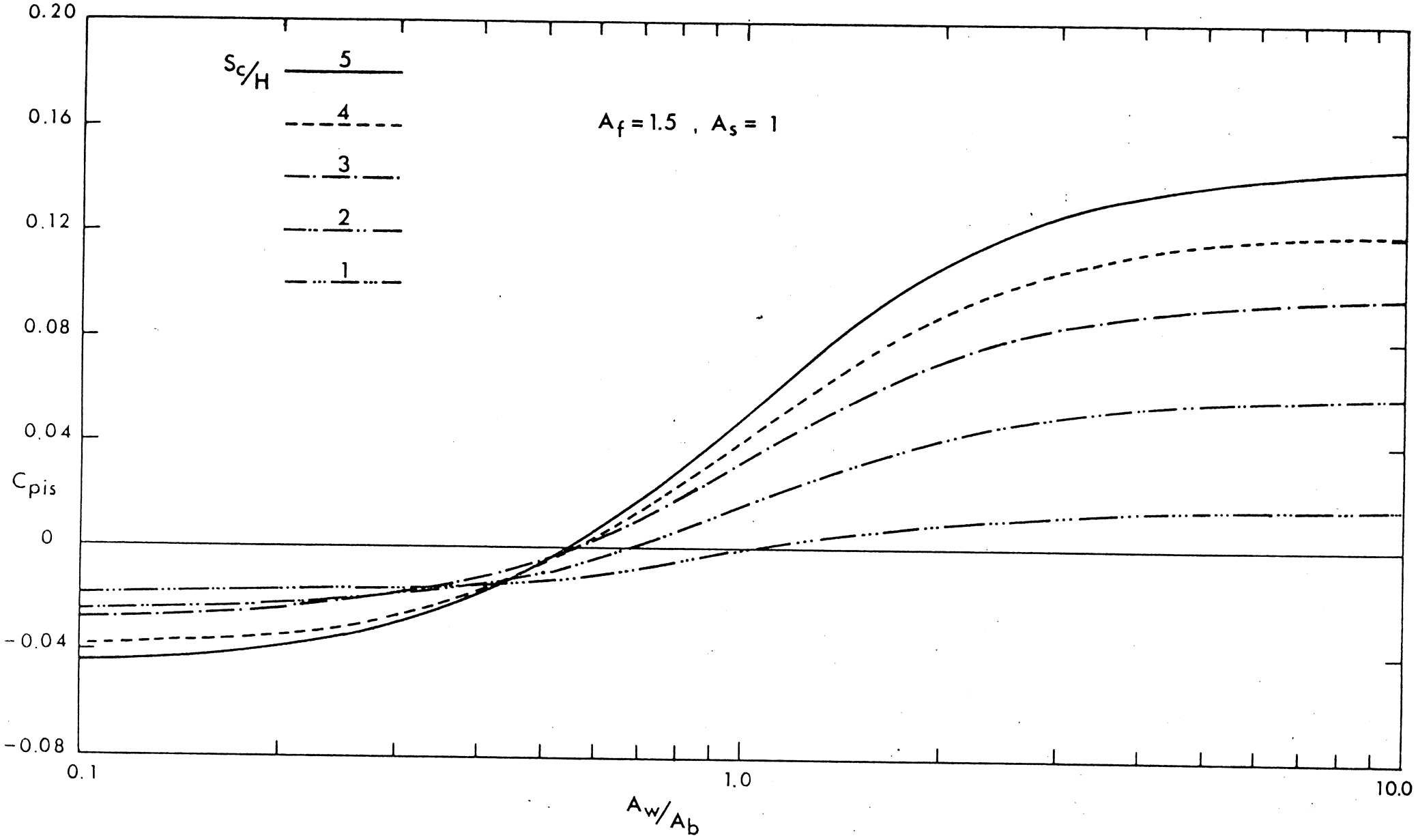

Figure A.3 The Variation of Internal Pressure Coefficient, Cpis, with Aperture Ratio, Aw/Ab for A_f = 1.5, A_s = 1.0.

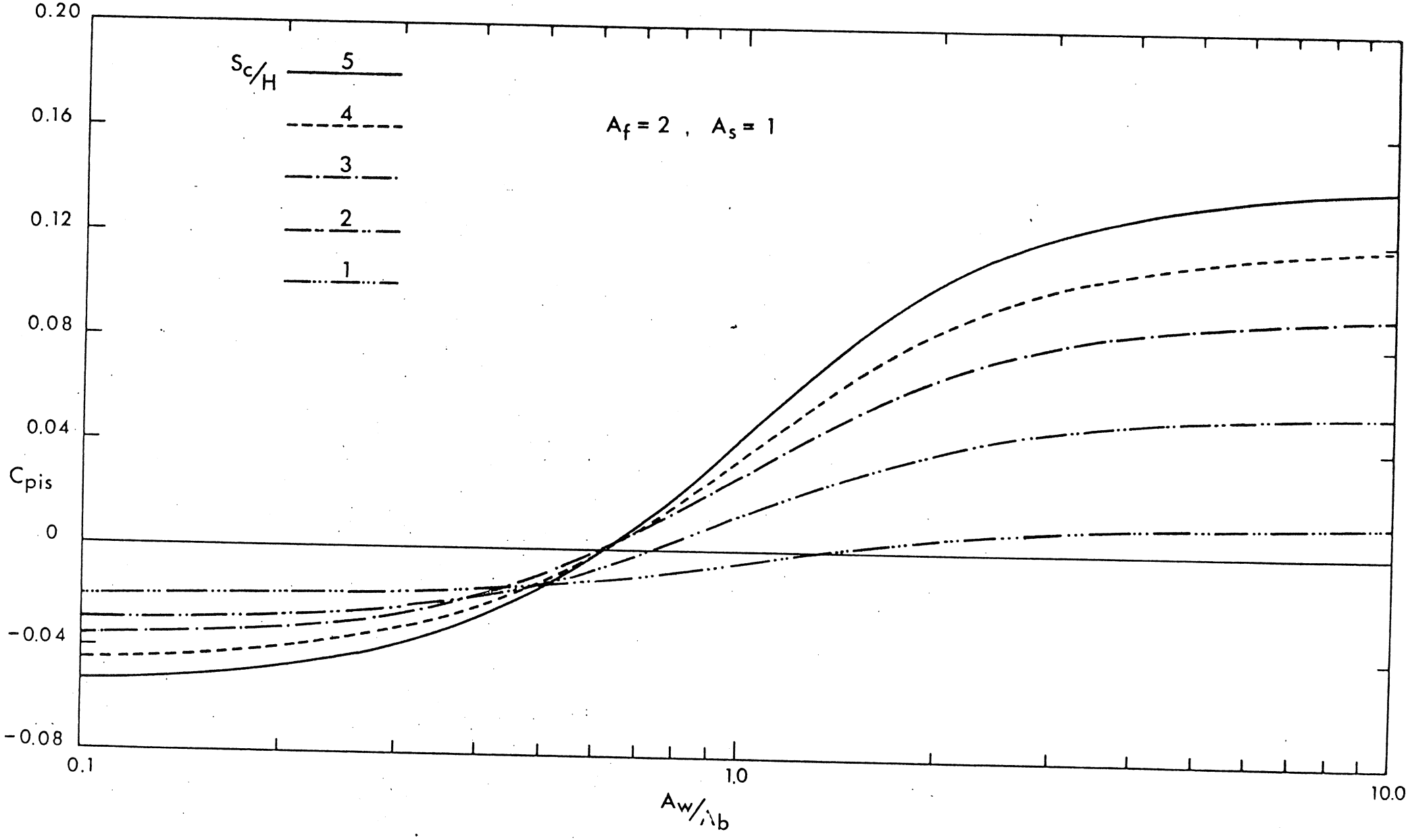

Figure A.4 The Variation of Internal Pressure Coefficient, Cpis, with Aperture Ratio, Aw/Ab, for A_f = 2.0, A_s = 1.0.

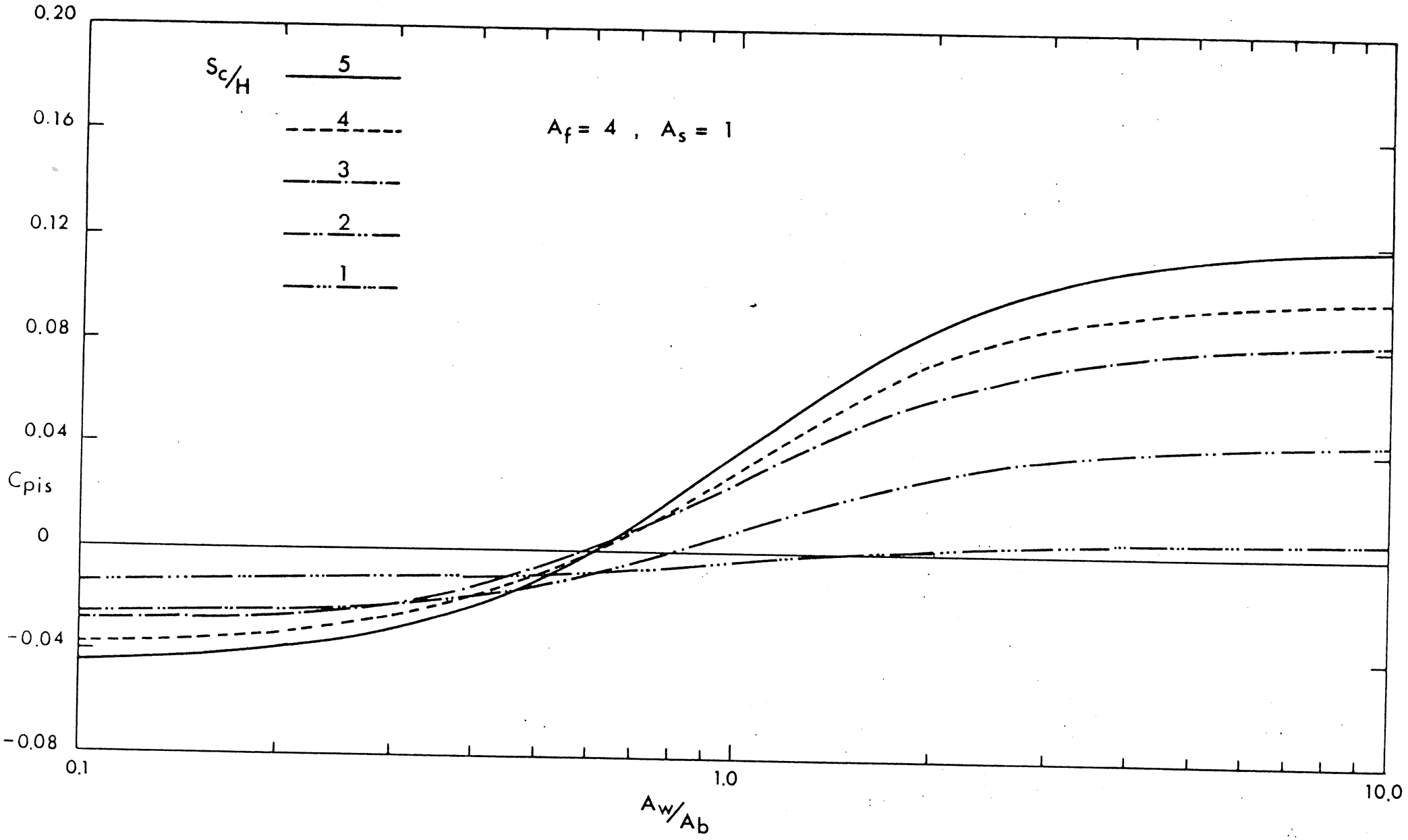

Figure A.5 The Variation of Internal Pressure Coefficient, Cpis, with Aperture Ratio, Aw/Ab for A_f = 4.0, A_s = 1.0.

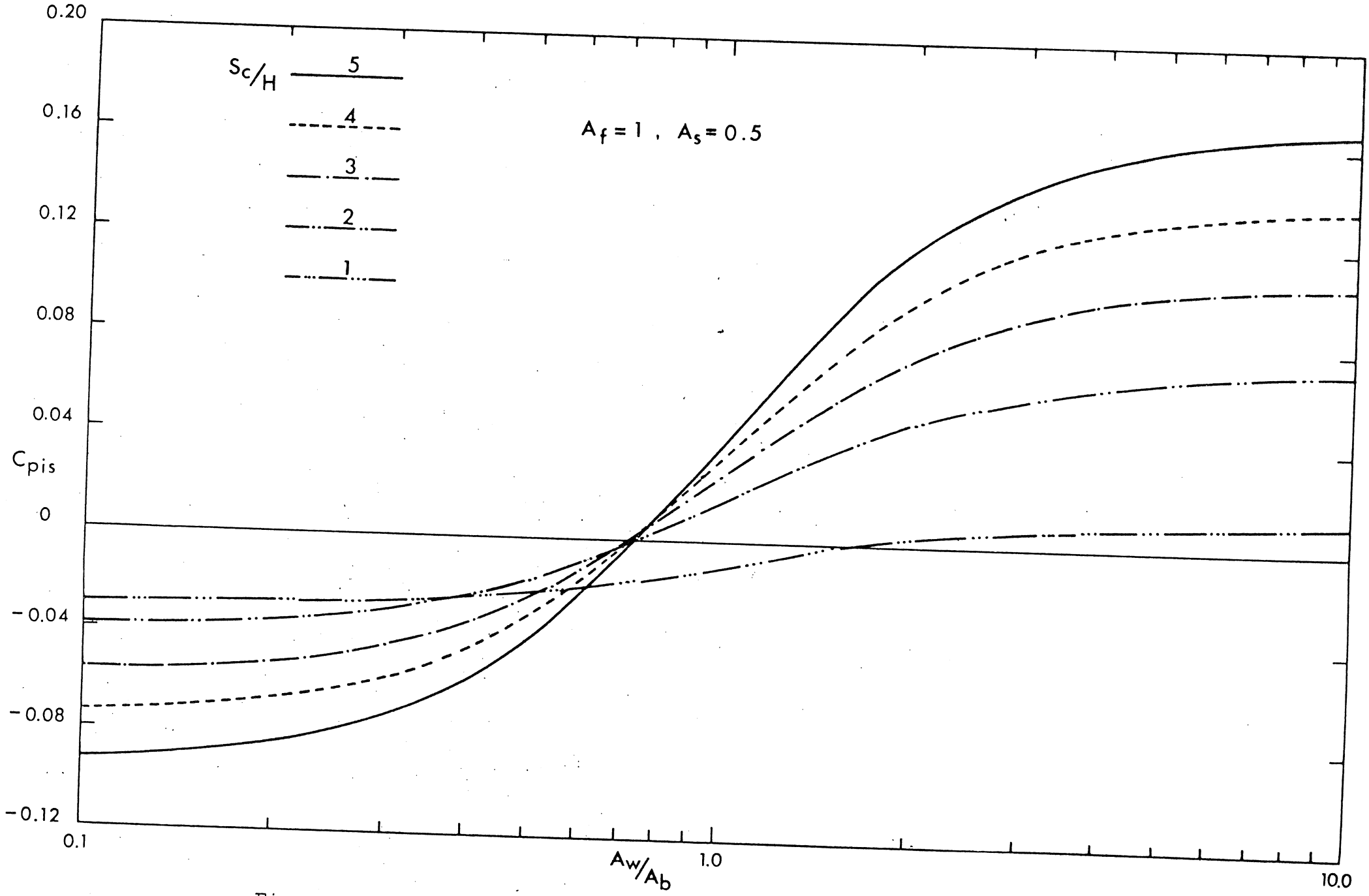

Figure A.6 The Variation of Internal Pressure Coefficient, Cpis, with Aperture Ratio, Aw/Ab for A_f = 1.0, A_s = 0.5.

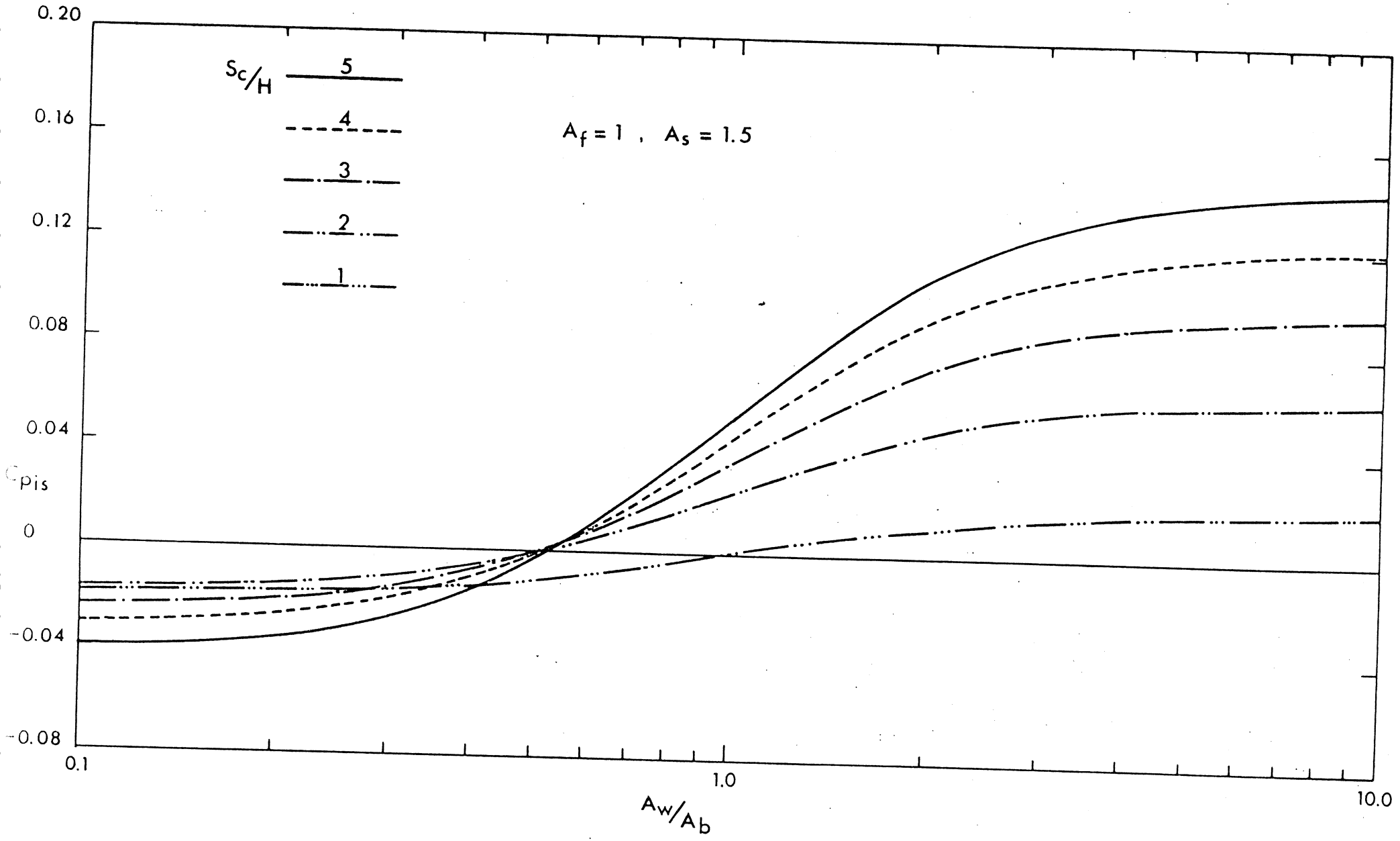

Figure A.7 The Variation of Internal Pressure Coefficient, Cpis, with Aperture Ratio, Aw/Ab for A_f = 1.0, A_s = 1.5.

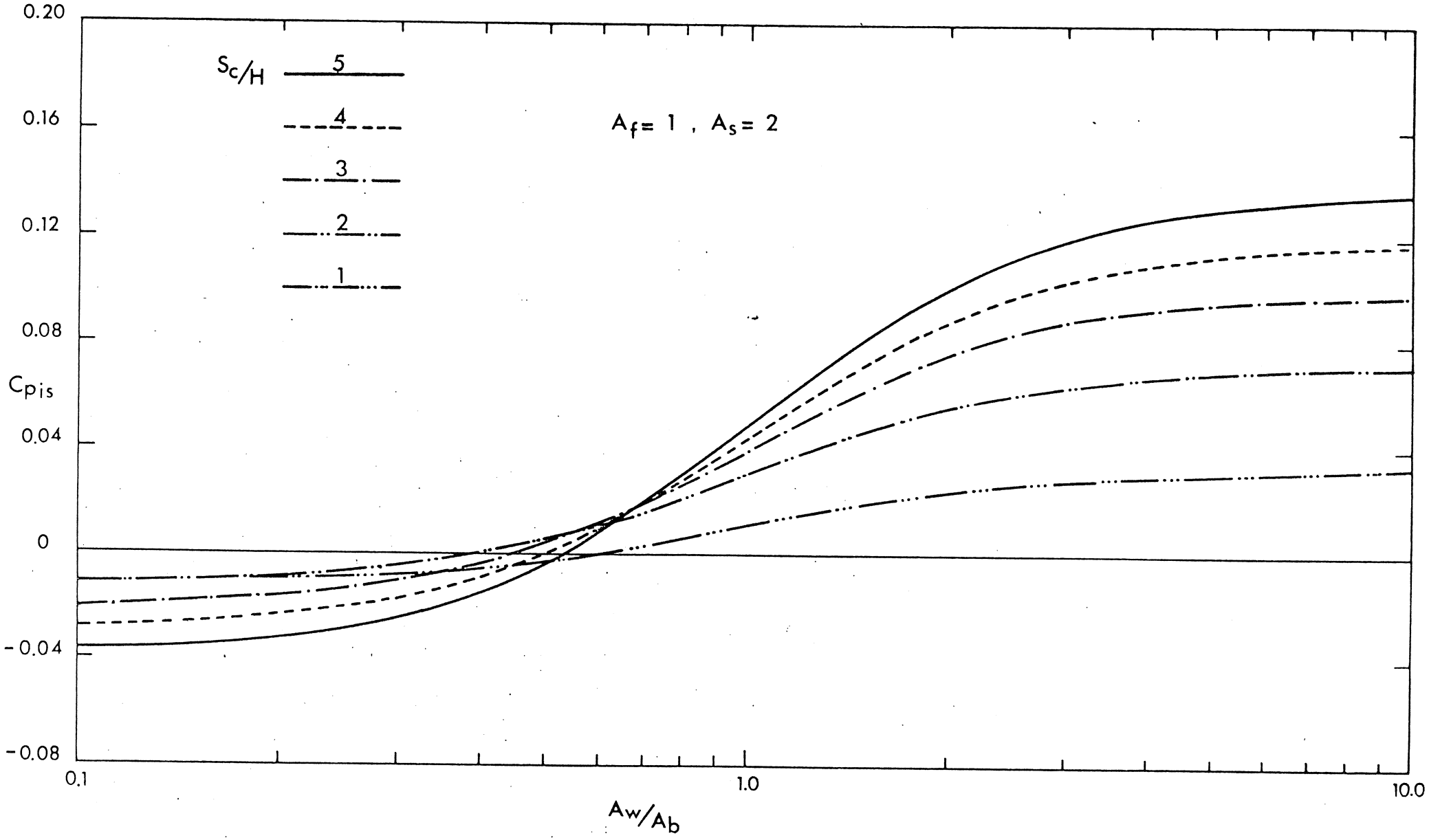

Figure A.8 The Variation of Internal Pressure Coefficient, Cpis, with Aperture Ratio, Aw/Ab for A_f = 1.0, A_s = 2.0.

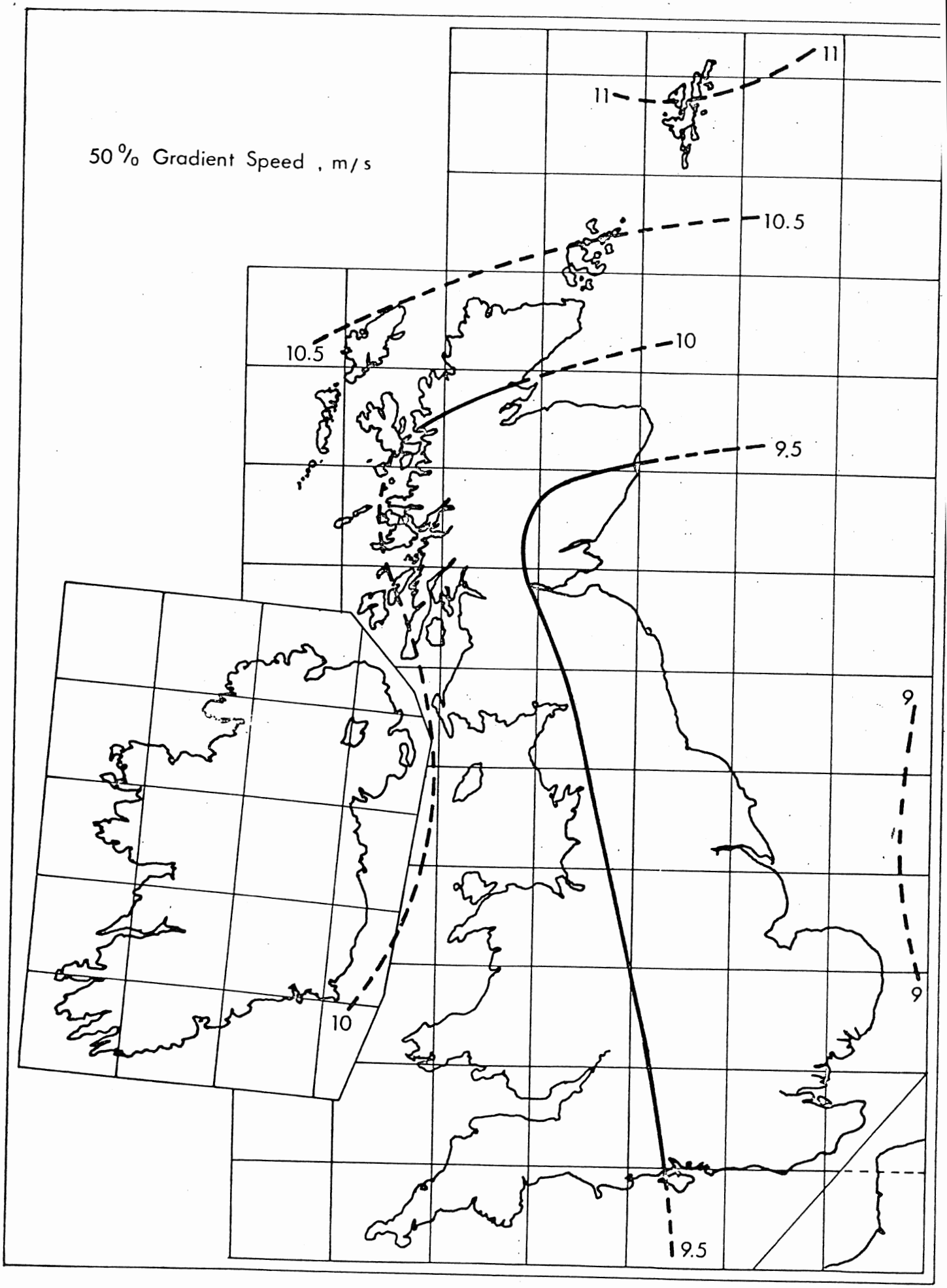

Figure B.1 Variation of Gradient Wind Speed over the United Kingdom. Speeds exceeded 50% of the time.

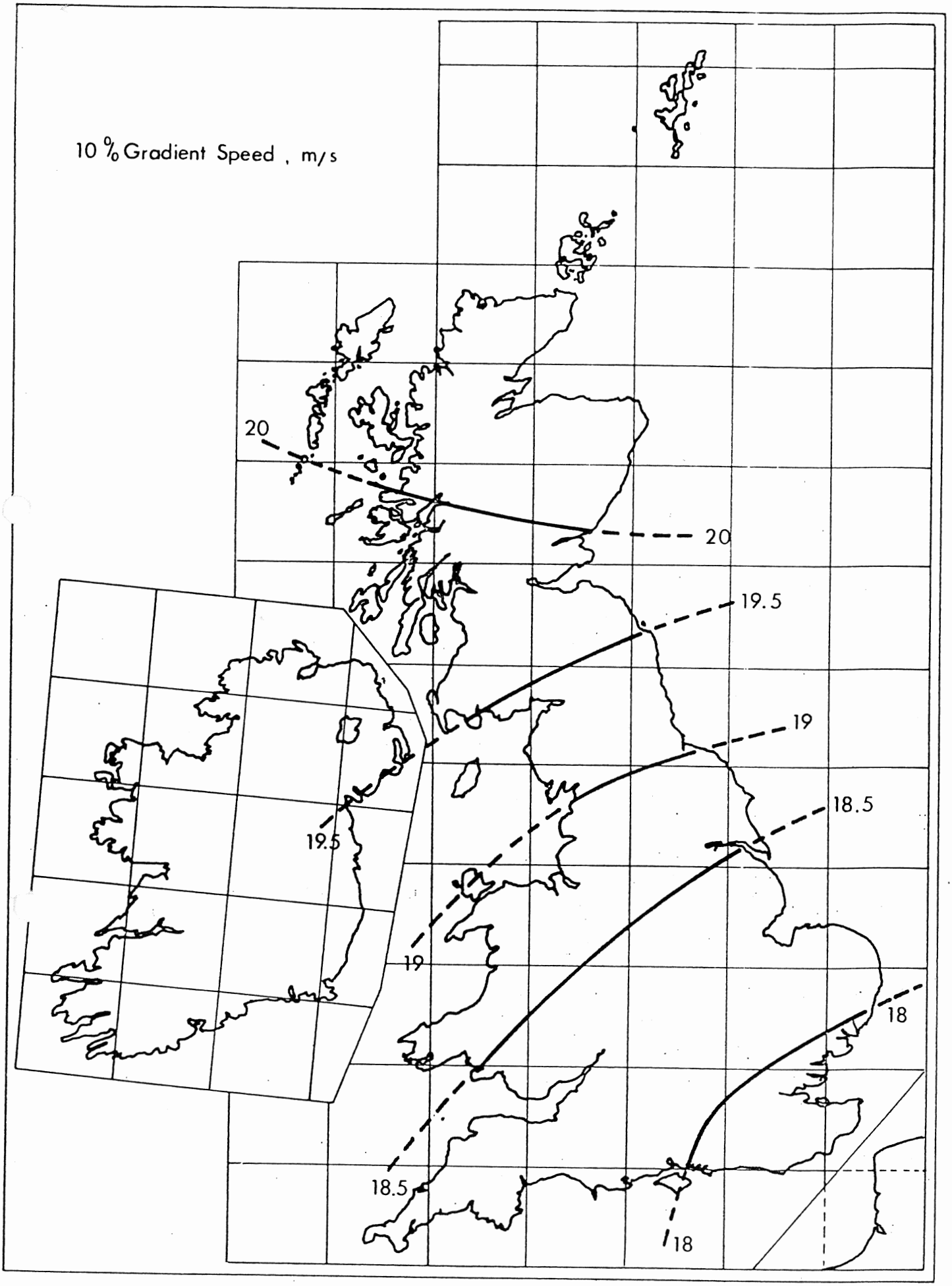

Figure B.2 Variation of Gradient Wind Speed over the United Kingdom. Speeds exceeded 10% of the time

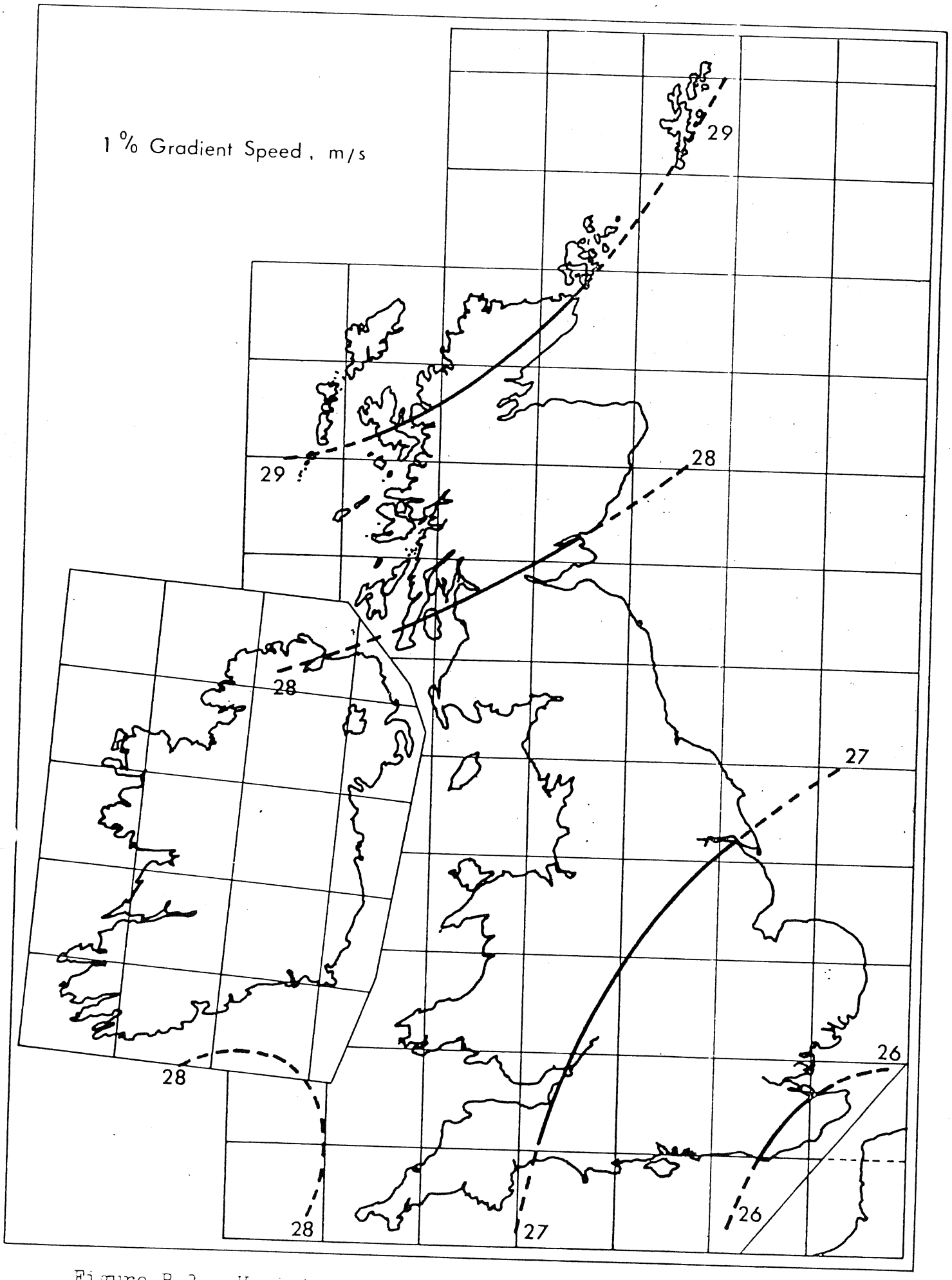

Figure B.3 Variation of Gradient Wind Speed over the United Kingdom. Speeds exceeded 1% of the time.